Stefan Luding

Towards Dense, Realistic Granular Media in 2D

Abstract The development of an applicable theory for granular matter – with both qualitative and quantitative value – is a challenging prospect, given the multitude of states, phases and (industrial) situations it has to cover. Given the general balance equations for mass, momentum, and energy, the limiting case of dilute and almost elastic granular gases, where kinetic theory works perfectly well, is the starting point.

In most systems, low density coexists with *very high density*, where the latter is an open problem for kinetic theory. Furthermore, many additional non-linear phenomena and material properties are important in realistic granular media, involving, e.g.:
(*i*) multi-particle interactions and elasticity
(*ii*) strong dissipation,
(*iii*) friction,
(*iv*) long-range forces and wet contacts
(*v*) wide particle size-distributions, and
(*vi*) various particle shapes.
Note that, while some of these issues are more relevant for high density, others are important for both low and high densities; some of them can be dealt with by means of kinetic theory, some can not.

This paper is a review of recent progress towards more realistic models for dense granular media in 2D, even though most of the observations, conclusions, and corrections given are qualitatively true also in 3D.
Starting from an elastic, frictionless and monodisperse hard sphere gas, the (continuum) balance equations of mass, momentum and energy are given. The equation of state, the (Navier-Stokes level) transport coefficients and the energy-density dissipation rate are considered. Several corrections are applied to those constitutive material laws – one by one – in order to account for the realistic physical effects and properties listed above.

S. Luding,
Multi Scale Mechanics, TS, CTW, UTwente,
P.O.Box 217, 7500 AE Enschede, Netherlands,
e-mail: s.luding@utwente.nl

Contents

1 Introduction

Interesting phenomena occur when granular materials move, as studied and reported during the last decades [1–37]. Of special interest is structure formation during free dissipative cooling of a granular gas [25, 38–54]. Starting from a homogeneous system, structures evolve and a dilute granular gas coexists with denser, possibly much denser and even solid-like clusters – in non-equilibrium. However, the coexistence of a fluid-like granular gas with a solid-like packing also occurs in many other systems, for example during avalanche flow on inclined planes or

in vibrated containers, see Refs. [28,30,32,34,55–59] and references therein. Methods developed for granular gases have even found application in the dynamics of animal encounters, see e.g. Ref. [60].

Granular materials form a "hybrid" state between fluid and solid. Besides the fact that fluid- and solid-like phases often coexist, the state of the granulate can easily change: For example, energy input can lead to dilatancy or fluidization, i.e., a reduction of density so that the material becomes 'fluid'. On the other hand, in the absence of energy input (e.g., through shear or vibration), granular materials densify or 'solidify' due to dissipation. This makes granular media an interesting non-linear multi-particle system with a rich phenomenology – sometimes fluid-like, sometimes solid-like – where the co-existence of both regimes allows for new and unexpected phenomena.

In the absence of walls and external forces, the crucial phenomena in a freely cooling granular gas involve the fluctuations in density, velocity and temperature, which cause position-dependent energy loss [38]. In denser areas, due to strong local dissipation, pressure and energy drop rapidly and material can move from 'hot' to 'cold' regions. Hence leading to even stronger dissipation and thus causing the density instability with ever growing (dense) clusters.

As a working example for granular systems, the freely cooling granular gas will be introduced first as a paradigmatic case where dilute and dense granular media coexist. Even though walls are avoided by periodic boundary conditions and the initial configuration is homogeneous, resembling a classical, elastic hard sphere gas, the system develops an interesting dynamics and structure formation – only due to the dissipative interactions of the particles, see Fig. 1 in section 2.

In brief, the paper is structured as follows: As an example, the transition from homogeneous to inhomogeneous cooling and cluster growth is introduced in section 2. As a starting point for a more realistic theory, a set of hydrodynamic equations is introduced in section 3, together with the classical constitutive relations and transport coefficients. In the rather technical section 4, the corrections for higher densities are reviewed in detail. A few special (simplified) cases of the hydrodynamic equations are reviewed in section 5. Several further corrections for realistic granular media are reviewed in section 6. Finally, sections 7 and 8 summarize and conclude the main results of this review paper, indicating the direction the author feels new research should be oriented.

2 From homogeneous to inhomogeneous cooling

When a homogeneous granular gas cools down due to collisional dissipation, one observes an initial homogeneous cooling state (HCS), followed by a cluster growth regime, and a final (inhomogeneous, non-equilibrium)

state where the cluster size is comparable to the system size, i.e., the structures span the whole system [38–47].

Using the hard sphere model and event driven simulations, see e.g. Refs. [61, 62], it is straightforward to simulate the time-evolution of a homogeneous granular gas with density (area fraction) $\nu = 0.25$, about $N = 10^5$ particles, and moderate dissipation with a coefficient of restitution $r = 0.9$.

2.1 Collision Model

For two particles, $p = 1, 2$, at positions $\mathbf{r}_{1,2}$, conservation of momentum leads to a collision rule:

$$\mathbf{v}'_{1,2} = \mathbf{v}_{1,2} \mp \frac{1+r}{2} \left(\hat{\mathbf{k}} \cdot (\mathbf{v}_1 - \mathbf{v}_2) \right) \hat{\mathbf{k}} , \qquad (1)$$

where a prime indicates the velocities $\mathbf{v}$ after the collision, and $\hat{\mathbf{k}} = (\mathbf{r}_2 - \mathbf{r}_1)/|\mathbf{r}_2 - \mathbf{r}_1|$ is the unit vector pointing along the line of centers, from particle 1 to particle 2.

At collision, the normal component, $v_n = \hat{\mathbf{k}} \cdot (\mathbf{v}_1 - \mathbf{v}_2)$, of the relative velocity, $\mathbf{v}_2 - \mathbf{v}_1$, changes its sign and is reduced by a factor $1 - r$, with the coefficient of restitution r. Therefore, the kinetic energy of the relative velocities normal component is reduced by the factor $\varepsilon = 1 - r^2$. The elastic limit, $r = 1$, implies no dissipation ($\varepsilon = 0$), while $r < 1$ implies $\varepsilon > 0$.

2.2 Free Cooling Granular Gas

Six snapshots at different (dimensionless) times, $\tau = t/t_n(0)$, with time t and initial collision rate $t_n^{-1}(0)$, are shown in Fig. 1. Different colors correspond to particles and white corresponds to "vacuum". The initial state is homogeneous with (arbitrary) collision rate around $t_n^{-1}(0) \approx 258\,\text{s}^{-1}$, which is only used to scale time in the following. The change in color from red to green and to blue indicates the decrease in non-dimensional collision rate, $\tau_n^{-1} = t_n(0)/t_n(t)$, due to the global cooling. The structures are growing with time, τ, and the collision rate inside the large clusters can become comparable to the initial collision rate.

The system evolution can be divided into three states: Firstly, the system is in the *homogeneous cooling state* (HCS) [2]. The decay of the kinetic energy and the collision frequency can be described by simple analytical expressions $E(\tau) \sim (1 + \tau)^{-2}$ and $f_c(\tau) \sim (1 + \tau)^{-1}$. The initial collision rate is used to make time and rate (frequency) dimensionless, however, the evolution of the system is controlled by the collision rate at the actual time, as discussed below in subsection 5.1.3.

After a few collisions per particle, *clusters begin to develop and grow* and the collision frequency can show large fluctuations in time because of cluster-cluster collisions. These cannot be quantitatively predicted anymore, even though the slower decay of energy can be predicted

$\tau = 0.024$

$\tau = 6.23$

$\tau = 99.66$

$\tau = 398.8$

$\tau = 1595$

$\tau = 12760$
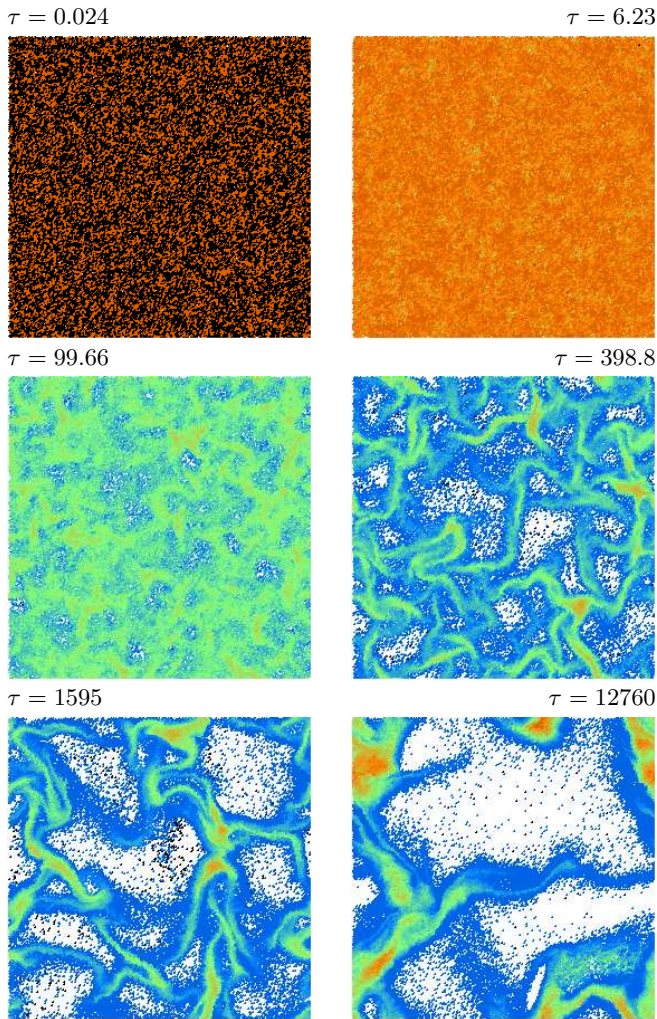
Fig. 1 ED simulation snapshots at different dimensionless times τ, from a two-dimensional (2D) system with $N = 99856$ particles, volume fraction $\nu = 0.25$, and coefficient of restitution $r = 0.9$. The collision frequency is color-coded: red, green and blue correspond to collision rates $\tau_n^{-1} \approx 1, 1/5$ and $1/25$, respectively. Black particles did not suffer a collision within the time interval $\tau/2$, different for each of the sub-plots, used to measure the collision rate. A critical collision frequency $\tau_c = 1/400$ was used (within the framework of the TC model as discussed below in subsection 6.2).

at early stages [63], before the clusters become too large. The energy decay is characterized by $E \sim \tau^{-1}$, with a power-law dependent on the situation. This regime shows interesting differences between two and three dimensions see [64, 65].

After many more collisions, most of the clusters merge to *one large cluster*, which grows until it reaches system size. Then the system behavior is dominated by the large cluster that contains a macroscopic fraction of the particles in the system, as specified in Ref. [64]. Kinetic energy and collision frequency still fluctuate, but are approximated by $E(\tau) \sim \tau^{-2}$ and $f_c(\tau) \sim \tau^{-1}$. This means the

evolution in time is similar to the homogeneous cooling state.

Inside the clusters, density can grow much larger than the global density while it drops to practically zero between the clusters. If the density grows above a certain (crystallization) limit the structure becomes an ordered (triangular in 2D) lattice. Crystallization happens frequently and cleanly in 2D, but is observed rarely (only locally) in the 3D systems examined.

3 Hydrodynamics

Assume a single-species multi-particle system, where the mass and momentum are conserved (microscopically) at each collision. The total mass and momentum are thus conserved macroscopically – which leads to macroscopic balance equations as introduced below. While mass and momentum are conserved, energy can be dissipated and inserted into the system, following certain rules. Making various assumptions [14, 66, 67], the constitutive relations and transport coefficients (occurring within the macroscopic equations for mass, momentum, and energy balance) can be derived [14, 67, 68]. Among these assumptions are scale separation [66, 69], molecular chaos [70, 71] velocity correlations [72], isotropy and disorder [73, 74], binary collisions [70, 75, 76], and many others, which will not be discussed in detail here.

3.1 Mass balance

Assume that N particles with total mass, $M = \sum_{p \in V} m^p$, are found in a certain representative volume element (RVE), with volume V. Mass-conservation implies that the mass-density, $\rho = M/V$, can only change with time by flux in or out of this RVE:

$$\frac{\partial \rho}{\partial t} + \frac{\partial}{\partial x_i}(\rho u_i) = \frac{D\rho}{Dt} + \rho \frac{\partial u_i}{\partial x_i} = 0 \ , \tag{2}$$

with the average streaming velocity components, $u_i = (1/M) \sum_{p \in V} m^p v_i^p$, where m^p is the particle mass, and v_i^p are the particles velocity components. The substantial derivative (or material derivative) is defined as: $\frac{D}{Dt} = \frac{\partial}{\partial t} + u_i \frac{\partial}{\partial x_i}$, where the sum over equal indices is implied. The second term in Eq. (2) involves the divergence of the velocity field and incompressibility would imply that it vanishes: $\frac{D\rho}{Dt} = \frac{\partial u_i}{\partial x_i} = 0$. However, since granular media are, in general, compressible the continuity equation (2) has to be considered completely.

3.2 Momentum balance

Momentum-conservation implies that the momentum density ρu_i can change with time, not only due to a (momentum carrying) flux $\rho u_i u_k$ in or out of the RVE, but

also due to inhomogeneous/directed forces (for example during collisions or due to gravity, γ_i) exerted from the outside on its interior:

$$\frac{\partial(\rho u_i)}{\partial t} + \frac{\partial}{\partial x_k}(\rho u_i u_k) = \rho \frac{Du_i}{Dt} = -\frac{\partial \sigma_{ij}}{\partial x_j} + \rho \gamma_i \,, \qquad (3)$$

with the first identity coming from Eq. (2), and the stress tensor components σ_{ij} on the right hand side. The stress can be split into an isotropic and a deviatoric part, $\sigma_{ij} = p^I \, 1_{ij} + \sigma_{ij}^D$, with (isotropic) pressure, p^I, and unit tensor 1_{ij}.

While the general balance equations are always correct, constitutive relations are not universal, but are required to proceed. For example, in the Euler case, all dissipative terms vanish, while in the isotropic case, the deviator stress vanishes. For a Newtonian fluid, the deviator stress is proportional to the deviatoric (shear) strain-rate (symmetric, trace-free velocity gradient):

$$\sigma_{ij}^D = -\eta \left[\frac{\partial u_i}{\partial x_j} + \frac{\partial u_j}{\partial x_i} \right] + \eta \frac{2}{\mathcal{D}} \frac{\partial u_k}{\partial x_k} 1_{ij} = -2\eta \hat{D}_{ij} \,, \qquad (4)$$

with the shear viscosity η and the deviatoric (symmetric) velocity gradient $\hat{D}_{ij} = (\partial u_i/\partial x_j + \partial u_j/\partial x_i)/2 - \frac{1}{\mathcal{D}}(\partial u_k/\partial x_k)1_{ij}$. Note, that the isotropic pressure, $p^I = p + p_\chi$, also contains a viscous term proportional to volume changes (divergence of the velocity field $\partial u_k/\partial x_k$), which are explicitly subtracted in Eq. (4), for $\mathcal{D} = 2, 3$ dimensions. The isotropic strain rate dependence of stress,

$$p_\chi = -\chi \frac{\partial u_k}{\partial x_k} \,,$$

contains an additional proportionality factor, χ, the bulk viscosity. The rate-independent pressure p will be considered, if not explicitly mentioned.

Note that the equation of state for p as well as the transport coefficients η and χ are proportional to non-linear functions of the density, which are very well predicted by kinetic theory for small and moderate densities. These functions are shown for the special case of a rigid hard sphere model in subsection 3.4.3.

For sake of brevity, here we neither discuss a possibly more involved dependence on temperature and other quantities, see e.g. [3, 77, 78], nor the possibility of additional (micro-polar) terms (like in the Cosserat approach [15, 79–86], see also Refs. [87–94] among many others), asymmetric terms in general, or the presence of anisotropy in the constitutive relations, e.g., for stress in Eq. (4), [73, 77, 95]. Some of these issues are addressed later in section 6.

3.3 Energy balance

The energy-balance involves the kinetic energy density, $\rho u^2/2$, due to the streaming velocity, u_i, where $u^2 =$ $u_i u_i$. In addition, there is also a fluctuating energy density, related to fluctuating velocity v_T and to the "granular temperature",

$$T = \frac{2E_{\mathrm{kin}}}{\mathcal{D}N} = \frac{1}{\mathcal{D}N} \sum_{p \in V} m^p \left(v_i^p - u_i \right)^2 = \frac{m_0 v_T^2}{\mathcal{D}} \,,$$

i.e., twice the fluctuating kinetic energy per particle per degree of freedom [1], where the sum runs over all N particles in the averaging volume V. The energy-density balance then reads:

$$\frac{\partial}{\partial t} \left(\frac{1}{2}\rho u^2 + \frac{1}{2}\rho v_T^2 \right) + \frac{\partial}{\partial x_k} \left[\left(\frac{1}{2}\rho u^2 + \frac{1}{2}\rho v_T^2 \right) u_k \right]$$
$$= -\frac{\partial}{\partial x_k} \left[u_i \sigma_{ik} + q_k \right] + \rho u_i \gamma_i - I + J \,. \qquad (5)$$

Computing the partial derivatives in Eq. (5) leads to terms that can be eliminated using Eqs. (2) and (3), so that energy balance simplifies to:

$$\frac{\rho}{2} \frac{D}{Dt} v_T^2 = \frac{\mathcal{D}N}{2V} \frac{D}{Dt} T = -\sigma_{ik} \frac{\partial u_i}{\partial x_k} - \frac{\partial q_k}{\partial x_k} - I + J \,, \qquad (6)$$

with the energy density dissipation rate, I, and the energy density input rate, J. The right hand side of Eq. (6) contains also the rate of shear-heating, and the divergence of the heat-flux. The latter contains the classical term proportional to the temperature gradient and the thermal conductivity, κ, and a second, non-classical term, proportional to the density gradient and the corresponding transport coefficient λ [14, 96–101], so that [2]:

$$q_k = -\kappa \frac{\partial T}{\partial x_k} - \lambda \frac{\partial n}{\partial x_k} \,.$$

The second term vanishes in systems with homogeneous density and one has $\lambda \to 0$ for almost elastic systems proportional to $(1-r) \to 0$. Like for the momentum balance equation (3) above, and the transport coefficients involved there, non-symmetry, anisotropy, and possible additional terms, are disregarded here, but should be kept in mind as possible extension to the present study.

3.4 The ("classical") transport coefficients

The basic philosophy of this review is to assume that the balance equations are complete/sufficient and that only the "classical" transport coefficients, known from kinetic theory, have to be changed to account for additional physics. Therefore, the "classical" transport coefficients for almost elastic systems up to moderate density are first introduced.

---

[1] Note that many authors define $T' = T/m_0$ as the granular temperature, which can lead to confusion, i.e., slightly different definitions and pre-factors, in the following.

[2] If $T' = T/m_0$ is used [25, 52, 54, 102], the thermal conductivity becomes $\kappa' = \kappa m_0$, and if the gradient of mass density, $\partial \rho/\partial x_k$, is used, one has $\lambda' = \lambda/m_0$.

Specifically, in the balance equations (2), (3) and (6), the $2+\mathcal{D}$ field quantities ρ, u_i, and $(\rho/2)\,v_T^2 = nT$, are referred to as the hydrodynamic fields, density, flux velocity (components), and fluctuating kinetic energy density, respectively. Note that the square-velocity tensor (related to the dynamic stress and to the granular temperature) is not necessarily isotropic, so that beyond Navier-Stokes order hydrodynamics, a tensorial temperature-like quantity might be necessary, together with higher order moments.

The equation of state for pressure, p, the viscosities, η and χ, the heat conductivity, κ, the density gradient pre-factor, λ, and the energy density dissipation- and input-rates, I and J, are referred to as transport coefficients in the following (for sake of brevity). They are, a-priori, variables that depend on the hydrodynamic fields and, possibly, also on their gradients or other terms, which are not considered or discussed here.

3.4.1 Transport coefficients in 2D

In two dimensions (2D), for a single species, in the elastic limit, $r \to 1$, in lowest order in powers of $1 - r^2$ and the gradients, the transport coefficients can be expressed, see, e.g., Refs. [14, 25, 52, 54, 73, 100, 102, 103], in terms of the granular temperature, T, and the volume fraction, $\nu = nV_0$, with the particle volume, $V_0 = \pi h d^2/4$, the particle mass, m_0, the number density, $n = N/V = \rho/m_0$, the particle (disk) height, h, and diameter, d:

$$p = nT\left(1 + 2\nu g(\nu)\right),$$

$$\eta = \frac{\rho d\sqrt{\pi T/m_0}}{8\nu g(\nu)}\left(1 + 2\nu g(\nu) + \left(1 + \frac{8}{\pi}\right)\left[\nu g(\nu)\right]^2\right),$$

$$\chi = \rho d\sqrt{\pi T/m_0}\left(\frac{2}{\pi}\nu g(\nu)\right),$$

$$\kappa = \frac{\rho d\sqrt{\pi T/m_0}}{2m_0\nu g(\nu)}\left(1 + 3\nu g(\nu) + \left(\frac{9}{4} + \frac{4}{\pi}\right)\left[\nu g(\nu)\right]^2\right),$$

$$I = nT\sqrt{\pi T/m_0}\frac{4}{\pi d}(1 - r^2)\nu g(\nu),$$

and J so far unspecified. Note that both I and J are not strictly bulk transport coefficients: while I represents a bulk-property, J could rather be seen as a boundary condition. The term λ before the density gradient in the heat-flux is not shown here, since it vanishes for $r \to 1$, but – for the sake of completeness – is shown in subsection 6.3.

3.4.2 Isolating the collisional momentum exchange

Using the "Enskog collision rate" (inverse time-scale):

$$t_E^{-1}(\nu, v_T) = \frac{8\nu g(\nu)v_T}{\sqrt{2\pi}d} =: \frac{v_T}{s(\nu)} ,\tag{7}$$

with $g(\nu) = g_2(\nu)$ as specified in Eq. (13) below, the thermal fluctuating velocity

$$v_T = \sqrt{2T/m_0} ,\tag{8}$$

and the free path,

$$s(\nu) = \frac{s_0}{\nu g(\nu)} , \quad \text{with} \quad s_0 = \frac{\sqrt{2\pi}d}{8}\tag{9}$$

allows us to rewrite the transport coefficients:

$$p = \frac{\rho^p \nu\, v_T^2}{2}\left(1 + 2\left[\nu g(\nu)\right]\right),$$

$$\eta = \frac{\rho^p \nu\, v_T s_0}{2\left[\nu g(\nu)\right]}\left(1 + 2\left[\nu g(\nu)\right] + \left(1 + \frac{8}{\pi}\right)\left[\nu g(\nu)\right]^2\right),$$

$$\chi = \rho^p \nu\left[\nu g(\nu)\right]v_T s_0\frac{8}{\pi},$$

$$\kappa = \frac{2\rho^p \nu\, v_T s_0}{m_0\left[\nu g(\nu)\right]}\left(1 + 3\left[\nu g(\nu)\right] + \left(\frac{9}{4} + \frac{4}{\pi}\right)\left[\nu g(\nu)\right]^2\right),$$

$$I = \frac{\rho^p \nu\left[\nu g(\nu)\right]v_T^3}{4s_0}(1 - r^2),\tag{10}$$

expressed in terms of the volume fraction, ν, the particle material density, ρ^p, the thermal velocity, v_T, the free path factor, s_0, and the collisional momentum exchange factor $G(r, \nu) = \frac{1}{2}(1 + r)\left[\nu g(\nu)\right]$, see subsection 6.3 for strong dissipation situations. In Eqs. (10) and in the following, the nearly elastic limit $r \to 1$ is considered, so that only the abbreviated form $G(\nu) := G(1, \nu) = \nu g(\nu)$ shows up.

In the low density limit, $\nu \to 0$, in leading order, the pressure becomes $p_0 = nT = \rho^p \nu v_T^2/2$, the viscosity is independent of density, $\eta_0 = \rho^p v_T s_0/2$, the bulk viscosity becomes $\chi_0 = \rho^p \nu^2 v_T s_0(8/\pi)$, the heat-conductivity is independent of density, $\kappa_0 = 2\rho^p v_T s_0/m_0 = 4\eta_0/m_0$, and the energy density dissipation rate becomes $I_0 = \rho^p \nu^2 v_T^3(1 - r^2)/(4s_0)$.

3.4.3 Isolating time-scale and mass density

We observe that, besides some constant factors, all transport coefficients are proportional to $\rho = \rho^p \nu$, to powers of v_T, and to powers of the product $G(\nu) = \nu g(\nu)$. If one extracts the combination ρt_E^{-1} from the transport coefficients, only powers of v_T and $G(\nu)$ remain as variables:

$$p = \rho\, t_E^{-1} v_T s_0\left(\frac{1}{2G(\nu)} + 1\right),$$

$$\eta = \rho\, t_E^{-1}\frac{s_0^2}{2}\left(\frac{1}{G(\nu)^2} + \frac{2}{G(\nu)} + \left(1 + \frac{8}{\pi}\right)\right),$$

$$\chi = \rho\, t_E^{-1}\frac{d^2}{4} = \rho\, t_E^{-1}\frac{8s_0^2}{\pi},$$

$$\kappa = \rho\, t_E^{-1}\frac{2s_0^2}{m_0}\left(\frac{1}{G(\nu)^2} + \frac{3}{G(\nu)} + \left(\frac{9}{4} + \frac{4}{\pi}\right)\right),$$

$$I = \rho\, t_E^{-1}\frac{v_T^2}{4}(1 - r^2),\tag{11}$$

hiding the implicit proportionality

$$\rho t_E^{-1} = \rho^p v_T \nu^2 g(\nu)/s_0 \propto v_T \nu G(\nu) .$$

This last form of the transport coefficients could allow us to transform time $t \to \tau = t\,t_E^{-1}$ and non-dimensionalize the balance equations, see Ref. [40, 63, 104, 105]. However, we will proceed with the transport coefficients as summarized in subsection 3.4.2.

3.4.4 Summary and general philosophy

As working hypothesis, for the rest of this review, we will (boldly) assume that the Navier-Stokes order Eqs. (2), (3), and (6) are complete and sufficient to describe arbitrary flow conditions and rheology. [3] Therefore, corrections or new effects have to be added as empirical terms to the "classical" transport coefficients from subsection 3.4.2 in Eqs. (10). *In the view of the author, applying these corrections is the first step, before generalizing the Navier-Stokes order equations. The corrections should (in the framework of a higher order theory) still remain valid.*

This ansatz implies, that the flow behavior of very dense, realistic granular matter can already be rather well described, in most cases, by *correcting the transport coefficients rather than the balance equations*. In the following, we will see how far we get with this idea, step by step, and postpone the introduction of more advanced theory to future studies – to the cases for which the approach proposed here does not work.

4 From low to high density

In the following, special cases of the balance equations are presented. The idea is to reduce complexity by reducing the number of relevant parameters for the transport coefficients and, ideally, to isolate a single transport coefficient. Firstly, in subsection 4.1, the equation of state of a homogeneous, elastic system in equilibrium is considered, so that only the pressure remains to be studied.

As a remark for the reader: Even though this section is quite technical, anyone who uses one of the many explicit forms of the 2D pair correlation function, which enters the equation of state and the transport coefficients, should be aware of their quantitative and qualitative differences, and specifically of their range of validity – for recent experiments, which show qualitatively good agreement, but some systematic quantitative deviations from the idealized hard sphere system data, see Refs. [110, 111].

4.1 Elastic 2D gas at all densities

In this subsection, the equation of state of a homogeneous, elastic system in equilibrium is considered. Vanishing time- and space-derivatives and $u_i = 0$, $\gamma_i = 0$, only leave the homogeneous pressure $p = nT(1 + 2\nu g(\nu))$ to be studied. The first term is the "ideal gas" contribution due to momentum transport by the translational fluctuating velocities. The second term accounts for the collisions of the particles and the related momentum transport. Since the density dependence of the first term is linear, we extract the dimensionless collisional pressure

$$P = p/p_0 - 1 = p/(nT) - 1 = 2\nu g(\nu) \,, \qquad (12)$$

which depends only on density but not on temperature for the hard sphere (HS) gas. The simulation results from a 2D system with periodic boundary conditions and $N = 1628$ particles, are plotted in Fig. 2 as circles. Additionally the different definitions of $g_\alpha(\nu)$ that are available in the literature are plotted for comparison, where the subscript α is used to identify the pair-correlation at contact or the non-dimensional collisional pressure $P_\alpha = 2\nu g_\alpha$. The discussion of the range of validity of the different pair correlation functions below is summarized in table 1.

Model	Eq.	Figs.	$\nu \ll 1$	$\nu < \nu_c$	$\nu \approx \nu_c$	$\nu > \nu_c$	ν_m
$g_1(\nu)$		2	x	≪	≪	≪	1
$g_2(\nu)$	(13)	2	X	X	>	<	1
$g_4(\nu)$	(14)	3	X	X*	>	<	-
$g_{2m}(\nu)$	(15)	2, 3	X	>	≫	≫	-
$g_{pm}(\nu)$	(17)	2–4	x	<	<	x<	x
$g_{sf}(\nu)$	(16)	2–4	>	<	<	x<	x
$g_{fv}(\nu)$	(18)	2–4	≫	>	<	X	X
$g_{dense}(\nu)$	(19)	4	≫	≪	<	X*	X
$g_K(\nu)$	(24)	4, 5	X	X	>	x>	x
$g_Q(\nu)$	(25)	4, 5	X	X*	*	X*	X

Table 1 Summary of the 2D pair-correlation functions at contact, as discussed and presented in this paper, with their range of validity when not under shear, where ν_c denotes the crystallization or fluidization density, see subsection 4.1.3. "Very good" quantitative agreement with HS simulations is indicated by an 'X', "good" agreement by an 'x', and the best fit to the data is indicated by a '*'. The terms "very good" and "good" mean error margins of much less and about one per-cent, respectively. The larger (>) and smaller (<) symbols indicate the direction of discrepancy. Not shown here are experimental data, e.g., Ref. [110, 111], and the interpolation proposed by Torquato et al. [112] for particles of different sizes.

---

[3] Note that additional terms up to Burnett-, super-Burnett-, or even higher orders [35, 66, 67, 69, 78, 96, 101, 106–109], are neglected as well as a possible micro-structure and anisotropy as, e.g., manifested in first normal stress differences [73, 77, 78].

4.1.1 Low and moderate densities

For mono-disperse hard disks in 2D (spheres [4]), the classical (Enskog) pair-correlation function at contact [5]:

$$g_2(\nu) = \frac{1 - 7\nu/16}{(1-\nu)^2} \; , \qquad (13)$$

leads to $g_1(\nu) \approx 1 + 25\nu/16$ in first order in ν, valid for very low densities. For low and moderate densities g_2 is in very good agreement with simulations, see Figs. 2 and 3. The disagreement at $0.5 \leq \nu \leq 0.6$ is between 1-2 per-cent (data not shown). Close to the fluid-density, $0.4 \leq \nu < \nu_c$, a higher order term [31,115–117],

$$g_4(\nu) = \frac{1 - 7\nu/16}{(1-\nu)^2} - \frac{\nu^3/16}{8(1-\nu)^4} \; , \qquad (14)$$

leads to even better agreement with simulations for $\nu \leq 0.67$. This defines $P_\alpha = 2\nu g_\alpha(\nu)$, with $\alpha = 1$, 2, and 4, as shown in Figs. 2-5. From Fig. 2, where g_2 and g_4 almost collapse with the data from simulations, *we conclude that for densities below $\nu \approx 0.5$ there is no reason to use any other g but $g_2(\nu)$*, since $g_4(\nu)$ only performs marginally better. Note that other $g_\alpha(\nu)$, as introduced below, can be qualitatively wrong and many are quantitatively wrong by at least 10-20 per-cent for intermediate, moderate densities, and thus should not be used in this density range.
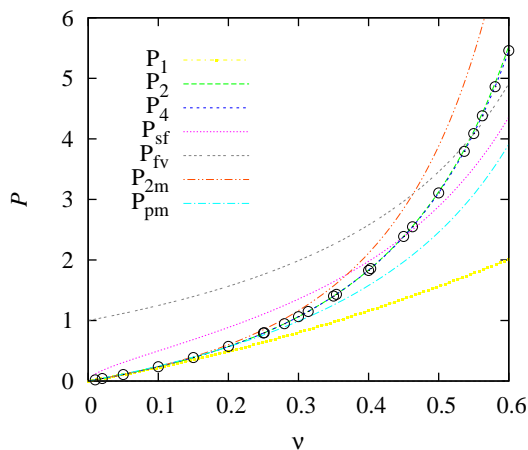
Fig. 2 (Color online) Dimensionless collisional pressure P with different variants of $g(\nu)$ (lines), as described in the main text, for low and moderate densities. Open symbols are 2D ED computer simulations from Ref. [116].

---

[4] When spheres are used in a quasi-2D geometry, some of the pre-factors in the transport coefficients have to be changed.

[5] – as proposed 1975 by Henderson [113] analogously to the Carnahan Starling function for 3D systems [114].

4.1.2 High densities

Granular materials at high densities show a hysteretic crystallization/melting transition in 3D [18,27,112,118–122] while hysteresis is much less apparent in 2D. The case of a two-dimensional vibrated granular gas at high density, where the liquid- and the solid-phases coexist, inspired a Fermi-type model [123]. This model enabled many predictions, for example, segregation in the presence of the condensed, dense phase [124]. The crystallization dynamics and rate dependence in 3D is still subject of research, as well as the question about the random packing density [27,122,125,126]. For recent theoretical and experimental data, see Refs. [127–129], where, e.g., the liquid-solid and solid-liquid transitions [129] are discussed in detail. In the following, however, we focus on the 2D situation.

For high densities, $\nu > \nu_c$, the above $g_2(\nu)$ and $g_4(\nu)$ fail to predict the HS numerical data, see Fig. 3, since they imply disorder and a maximal density $\nu_m = 1$ (data not shown), where pressure diverges. Around the crystallization density, ν_c, the pressure drops considerably due to ordering effects, as shown below in Fig. 5. Particles in an ordered configuration have longer free path to travel and therefore both collision rate and pressure are smaller than predicted by g_2 or g_4.

Due to excluded volume effects the pressure diverges (with a power law with exponent -1) at a lower density, $\nu_m = \pi/(2\sqrt{3})$, the closest possible packing density of hard spheres/disks in 2D, arranged on a triangular lattice. Therefore, in the attempt to describe the pressure correctly at high densities, up to ν_m, several expressions for the non-dimensional pressure were proposed, see [31,115,116,130] and references therein. One attempt to correct $g_2(\nu)$ [113,131] as

$$g_{2m}(\nu) = \frac{1 - 7\nu/16}{(1 - \nu/\nu_m)^2} \; , \qquad (15)$$

only performs at very low densities, but does neither perform at intermediate nor at high densities, see Fig. 3, due to the wrong power-law divergence with power -2. This also excludes other formulations with powers different from -1 and leads us to discourage the use of Eq. (15). However, different power laws were, to our knowledge, typically reported in very different situations concerning particle interactions and boundary conditions. Therefore, here, we can only say something about the almost elastic, homogeneous case without shear, and not about other situations with, for example, strong dissipation, see Ref. [132], where a different power law was reported. Nevertheless, some simulations suggest a wider range of validity of the constitutive relations, e.g., for inhomogeneous systems under shear [52,54].

Other formulations of $g_\alpha(\nu) = P_\alpha/(2\nu)$, are:

(*i*) free-volume forms with a square-root function of density, from more than 50 years ago [133, 134]:

$$P_{\rm sf} = \frac{1}{1 - \delta/\delta_m} = \frac{1}{1 - \sqrt{\nu_m/\nu}} \;, \qquad (16)$$

with typical particle distance, δ, closest distance, δ_m, and 2D volume fraction $\nu \propto \delta^{-2}$, see Refs. [115, 116, 133, 135, 136].

(*ii*) an interpolation form proposed by Grossman et al. see Eq. (8) in Ref. [137],

$$P_{\rm pm} = \frac{\nu_m + \nu}{\nu_m - \nu} - 1 = \frac{2\nu}{\nu_m - \nu} \;, \qquad (17)$$

which has the nice property that it also predicts the dilute limit.

(*iii*) the high density limit ($\nu \to \nu_m$) of Eq. (17),

$$P_{\rm fv} = \frac{2\nu_m}{\nu_m - \nu} - 1 = \frac{\nu_m + \nu}{\nu_m - \nu} = P_{\rm pm} + 1 \;, \qquad (18)$$

see Refs. [115, 116, 130], which is evidently wrong at low densities.
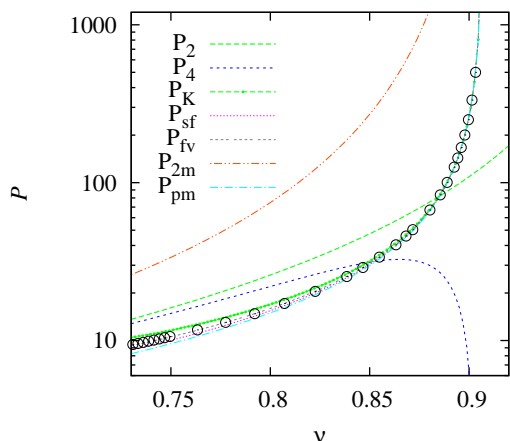
Fig. 3 (Color online) Dimensionless collisional pressure P with different variants of $g(\nu)$ (lines), as described in the main text, for high densities. Open symbols are 2D ED computer simulations [116].

The forms $P_{\rm sf}$, $P_{\rm pm}$, and $P_{\rm fv}$, indeed all collapse well with the HS data at very high densities, see Fig. 3. Note that deviations of a few percent at $\nu \approx 0.75$ are hardly visible in this logarithmic plot.

The equations of state $P_{\rm sf}$, Eq. (16), $P_{\rm pm}$, Eq. (17), and $P_{\rm fv}$, Eq. (18), all approximate well the pressure at maximal density, but at $\nu \approx 0.75$, already deviate by 5%, 10% and $< 1\%$, respectively. The former two deviating about linearly in $\nu_m - \nu$. Thus, *if exclusively high densities $\nu > 0.75$ are considered, $P_{\rm fv}$ should be used* – for lower densities $P_{\rm fv}$ is wrong and thus not recommended.

Two remarks about $P_{\rm pm}$, which is frequently used in literature [55, 57, 138] instead of the more appropriate forms [56, 112, 115].

(*i*) Eq. (17) has the big advantage, that it behaves qualitatively correct for *all* densities – including the limits of low and high density – even though it has considerable deviations from the HS simulation reference data at intermediate densities, see table 1 and Figs. 2-4.

(*ii*) If one adds unity to Eq. (17), the collisional pressure becomes $P_{\rm fv} = P_{\rm pm} + 1$, with better quality at high density – but deteriorating at low density. [6]

The only equation of state known to us that is concise – and involves the low as well as the high density limits – is Eq. (17). Due to its compactness, it might even allow for analytical solutions of some problems. Unfortunately, there is no hope for quantitative agreement with HS simulations.
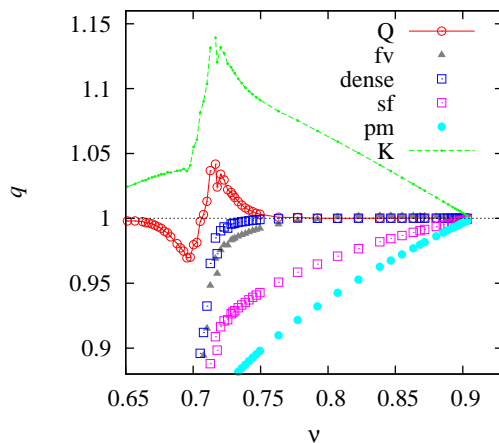
Fig. 4 (Color online) Quality factor of different equations of state $q = P_\alpha/P_{\rm sim}$, where α is given in the inset and $P_{\rm sim}$ are the values from 2D ED computer simulations [116].

Before we propose a "global equation of state" [115, 116, 139] [7] that is in best quantitative agreement with our simulation results for all densities, we first correct $P_{\rm fv}$ by an empirical fit

$$P_{\rm dense} = \frac{2\nu_m}{(\nu_m - \nu)} \, h(\nu_m - \nu) - 1 \;, \qquad (19)$$

with $h(x) = 1 + c_1 x + c_3 x^3$, and the fit parameters $c_1 = -0.04$, and $c_3 = 3.25$ [116]. The formulation $P_{\rm dense}$ performs very well for $\nu > 0.75$, with agreement much better than 0.1% when compared to the simulations.

---

[6] The addition of unity might be a source of confusion, since we discuss the collisional pressure here and the term unity corresponds to the dynamic pressure due to the fluctuating kinetic energy. Thus, in order to avoid miss-understandings, we note that the dimensional full pressure is $p = nT(1 + P_\alpha)$, and $\alpha = {\rm fv}$ is recommended for high densities only.

[7] The phrase "global" means here that the equation of state is valid for all densities. This is not to be confused with a local, vs. a global validity: The present results are supposed to be locally valid, *not* globally [139].

4.1.3 Densities around ν_c

Up to now, the equations of state discussed perform either at low and moderate densities, or at high densities. The inspired and compact interpolation Eq. (17) is unfortunately about 20% wrong for intermediate densities and thus does not have quantitative predictive value.

Therefore, an interpolation was proposed [115, 116], using the merging function

$$m(\nu) = [1 + \exp(-(\nu - \nu_c)/m_\nu)]^{-1}, \qquad (20)$$

with center $\nu_c = 0.699$ and width $m_\nu = 0.0111$, which leads to

$$P_Q = P_4 + m(\nu)[P_{\mathrm{dense}} - P_4], \qquad (21)$$

i.e., the global equation of state [75, 115, 116]. Note that the choice of ν_c and m_ν allows the adjustment of the behavior of P_Q in the transition regime. In the literature one can find slight variations in the values, dependent on the details of the fits and the criteria used to obtain them. (For example, $\nu_c = 0.7010$, 0.7006, or 0.7000 are reported – while, above, we shifted the transition density to slightly smaller values, $\nu_c = 0.6990$.) The global equation of state, P_Q, is valid for all densities, with an error margin smaller than 0.1%, besides stronger deviations, of order of 1%, in the transition regime. These are because – like for the Maxwell-construction in thermodynamics [134] – a positive slope of $P(\nu)$ was enforced, see Figs. 4 and 5.

Somewhat simpler forms of the global equation of state, already discussed in Refs. [115, 116], are still in good agreement with the simulation data for most densities. Here we explicitly report the recently introduced (also simpler) form of Khain [52, 54]:

$$P_K = P_2 + m(\nu)[P_{\mathrm{fv}} + 1 - P_2], \qquad (22)$$

with $\nu_c = 0.70$ and $m_\nu = 0.0111$, where the addition of unity comes from disregarding the subtraction of unity in Eq. (18). For large densities this is indeed negligible, but for densities around 0.75, it is a 10% overestimation of P_{fv} and thus of the reference simulations [115, 116] – the opposite of the about 10% underestimation when using P_{pm}.

However, as a cautionary note: The simulation data in Refs. [115, 116] were obtained by starting from a perfect 2D-crystal structure and very slowly reducing the density. As a guess, when starting from low densities and increasing the density to higher values $\nu_c < \nu \approx \nu_m$, one expects an increased pressure and the divergence at a lower ν_m, due to the frozen-in disorder (a few defect-lines and isolated defects). Therefore, P_K from Eq. (22) might in practice even perform better than P_Q from Eq. (21). The very good agreement of shear simulations with the corresponding continuum predictions using P_K supports this [52, 54]. The truth probably lies between (or around) the two forms P_Q and P_K in many dynamic situations.
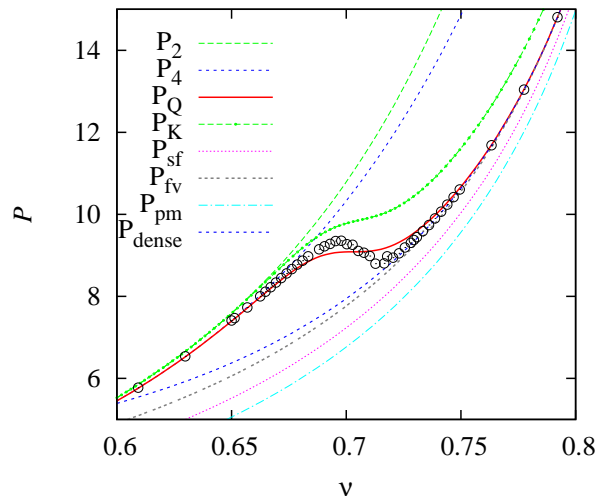
Fig. 5 (Color online) Dimensionless collisional pressure P in different variants as described in the main text for moderate densities. The solid red line is the "global equation of state" for 2D that fits simulation data best for all densities. P_2 and P_4 are plotted in green and blue, respectively.

All non-dimensional collisional pressures P_α can be translated into the pair-correlation functions at contact

$$g_\alpha(\nu) = \frac{P_\alpha}{2\nu} . \qquad (23)$$

Especially the forms [52]:

$$g_K(\nu) = \frac{P_K}{2\nu} = g_2 + m(\nu)[g_{\mathrm{fv}} + 1/(2\nu) - g_2], \qquad (24)$$

and [115]:

$$g_Q(\nu) = \frac{P_Q}{2\nu} = g_4 + m(\nu)[g_{\mathrm{dense}} - g_4], \qquad (25)$$

are explicitly given here and – together with all others – are summarized in table 1.

4.1.4 Consequences for other transport coefficients

Since $g_Q(\nu)$ is obtained from the collisional pressure, it also describes the collision rate at all densities, see Eq. (7) and Fig.1 in Ref. [52]. Consequently, see [24, 52], we propose to set all $g(\nu) = g_Q(\nu)$ in all transport coefficients in subsection 3.4.

Therefore, $g(\nu) = g_Q(\nu)$ will be used in Eqs. (10) and (11), respectively, see [24, 52, 75, 115, 116, 140]. This leads to different expressions not only for the pressure but also for all other transport coefficients, as discussed in the next subsection 4.2.

4.2 Improved transport coefficients

In this subsection, we discuss the consequences of using different $g \neq g_2$ in the transport coefficients.

As empirical extrapolation, based on the global equation of state, P_Q and the global pair-correlation at contact, g_Q, we propose to generalize also the other transport coefficients by setting $g = g_Q$. As shown below this leads to plausible forms of the transport coefficients. Note that the viscosity behaves qualitatively in a different way, see Refs. [21, 24, 52, 54, 141], as discussed below in subsection 4.2.4.

4.2.1 Energy dissipation rate

The energy dissipation rate [8] is proportional to the collision rate – as discussed in the previous subsection. Like the collisional pressure, the dissipation rate I vanishes proportional to ν^2 for $\nu \to 0$.

When scaling either the collision rate or the energy dissipation rate by the respective low density limit, one gets $g_\alpha(\nu) = t_E(\nu \to 0)/t_\alpha = P_\alpha/P_0 = I_\alpha/I_0$ as displayed in Fig. 6 for different α. Therefore, it is straightforward to replace g by g_Q or g_K, which leads to the new energy dissipation rates $I_\alpha = I_0 g_\alpha$. For some more detailed discussion see the next subsection 4.2.2.

4.2.2 Bulk viscosity

For the (isotropic) bulk viscosity χ, see Eq. (10), as plotted in Fig. 6, inserting g_2 or g_4 does not make a visible difference for low densities, but both forms must fail for high densities due to the wrong maximal density. The interpolation form g_{pm} shows considerable disagreement with the "classical" χ_2 for intermediate and very low densities, and thus is not recommended, even though it shows the plausible divergence at high densities.

Only g_Q or g_K lead to a plausible χ (and I) for all densities – including the wiggle around $\nu_c \approx 0.7$. Note the slightly negative slope for g_Q (which might cause practical numerical problems) is avoided when using g_K.

4.2.3 Heat conductivity

For the heat conductivity κ, see Eq. (10), as plotted in Fig. 7, inserting g_2 or g_4 does not make a visible difference for low densities, but both forms must fail for high densities due to the wrong maximal density. The interpolation form g_{pm} shows considerable disagreement with the "classical" κ_2 for intermediate and very low densities, and thus is not recommended, even though it shows the plausible divergence at high densities.

Using g_Q leads to a plausible κ_Q for all densities – including the wiggle around $\nu_c \approx 0.7$. Interestingly, replacing g_Q by g_2 in the second (third) term of κ_Q leads to good (bad) behavior. This shows that the third term of κ_Q is dominant in the high density regime.

---

[8] I is not really a transport coefficient in the strict sense, however, it is named as such, in combination with the other transport coefficients, for the sake of brevity
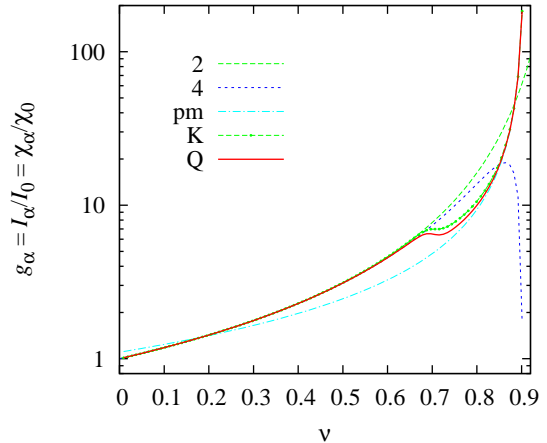
Fig. 6 2D pair correlation function at contact which is identical to the dimensionless energy dissipation rate I_α/I_0, and the dimensionless bulk viscosity χ_α/χ_0, where α is the abbreviation given in the inset, and χ_0 is the low density limit of χ in Eq. (10). The solid red and green lines give the "global equation of state" for both energy dissipation rate and bulk viscosity, involving $g = g_Q$ or g_K, while the other curves involve g_2, g_4, and g_{pm} (light-blue).

Using κ_Q instead of κ_2 was already proposed in Ref. [24] due to a slightly better agreement with (rather noisy) numerical data. Different variations of κ were also used and compared in Ref. [131].

As observed by Garcia-Rojo et al. [24], the simulation data for κ are higher than expected from the κ_2 prediction – already for rather low densities. Therefore, an empirical correction was proposed [52, 54]:

$$\kappa_K = \kappa_{2 \to K} \left\{ 1 + \frac{\nu}{10} - 10\,\nu^{10} + 0.11 \frac{\nu/\nu_m}{\nu_m - \nu} \right\} , \quad (26)$$

with $\kappa_{2 \to K}$ obtained by replacing all g_2 by g_K, instead of the original κ_2 [52]. We propose to replace the above fit by another (likewise empirical) correction:

$$\kappa_L = \kappa_Q \left\{ 1 + 0.15\,\nu^{1/2} \right\} , \quad (27)$$

which contains the reduction of κ for $\nu > \nu_c$ intrinsically through κ_Q and therefore remains much shorter/simpler. As a final remark, zooming into the transition zone shows that none of the variants of κ has a negative slope.

In conclusion, the reason for the somewhat larger heat-conductivity observed in simulations [24] remains an open question. Future new simulations with larger systems and in sheared or other inhomogeneous situations will allow us to better judge which form of κ is most appropriate.

4.2.4 Viscosity

The shear viscosity, when inserting different g_α, behaves qualitatively similar to the heat-conductivity, see subsection 4.2.3 above. Also the third term dominates for high
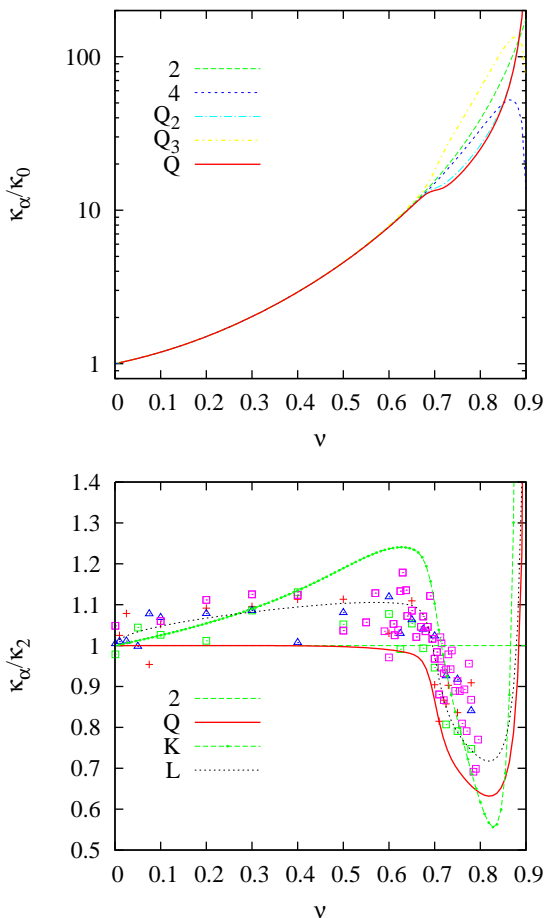
Fig. 7 (Top) Dimensionless 2D heat-conductivity κ_α/κ_0, where α is the abbreviation given in the inset, and κ_0 is the low density limit of κ in Eq. (10). The solid red line gives the "global equation of state" for heat-conductivity, involving $g = g_Q$, while the other curves involve g_2, and g_4. The curves indexed Q_2 and Q_3 represent κ_Q with g_2 in either the second or third term. (Bottom) Heat conductivity scaled by the "classical" Enskog prediction κ_2 in the high density regime. The curves with index K and L correspond to the corrections in Eqs. (26) and (27). The symbols give the simulation results from Ref. [24], see also Fig. 8.

densities and, like κ_Q, also η_Q does not have a negative slope.

However, when comparing η_Q to the simulation data from Refs. [21,24] in Fig. 8, a strong discrepancy between measured viscosity and Enskog prediction becomes evident [9] that was described/fitted by the correction factor:

$$\frac{\eta_R}{\eta_E} = 1 + \frac{c_\eta}{\nu_\eta - \nu} \ , \tag{28}$$

with $c_\eta = 0.037$ and a divergence at $\nu_\eta = 0.71$.

---

[9] The data in Ref. [24] were obtained in a homogeneous, elastic configuration without shear, whereas the data in Ref. [21] were obtained in a Poiseuille flow configuration at fixed temperature.
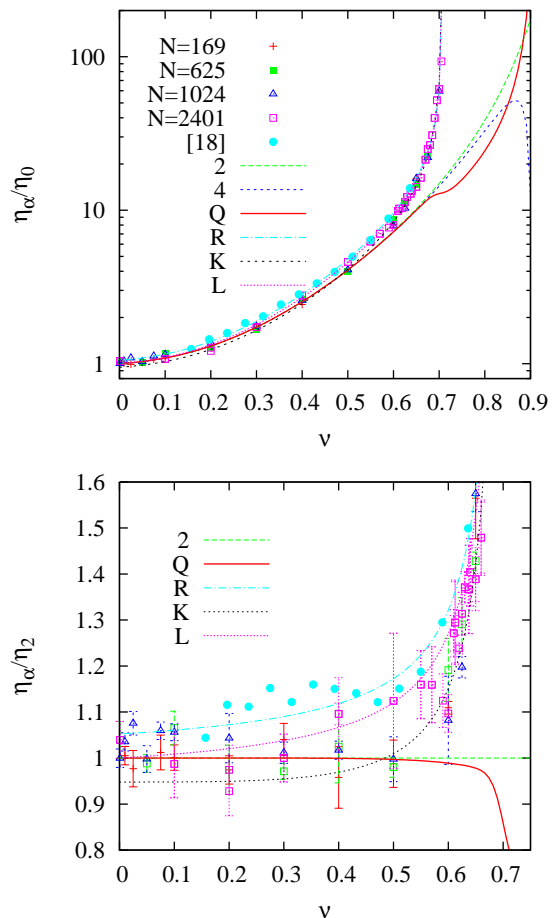
Fig. 8 (Top) Dimensionless 2D viscosity η_α/η_0 and (Bottom) scaled by the Enskog prediction η_α/η_2, plotted as function of density. The solid line gives the "global" viscosity, involving $g = g_Q$, while the other curves involve g_α as above in Fig. 7. Symbols are the simulation data from Refs. [24] and [21]. The empirical correction functions proposed in Refs. [24] and [52], are denoted as R and K, respectively – the new formula in Eq. (30) is denoted by L.

An alternative fit was proposed in Ref. [52]:

$$\frac{\eta_K}{\eta_E} = 1 + \frac{c_\eta(\nu/\nu_\eta)^3}{\nu_\eta - \nu} - \frac{c_\eta}{\nu_\eta} \ , \tag{29}$$

involving a modified, density dependent pre-factor. In a more recent paper [54] the last term is removed, which improves the low density regime but has no big effect for large densities. Here, we propose a new form that combines simplicity and the correct limit for $\nu \to 0$:

$$\frac{\eta_L}{\eta_Q} = 1 + \frac{c_\eta}{\nu_\eta - \nu} - \frac{c_\eta}{\nu_\eta} \tag{30}$$

as displayed in Fig. 8. Note that using η_2 or η_Q does not matter much for the viscosity since their small difference for $\nu < \nu_\eta$ is much smaller than the correction due to the term that diverges at ν_η.

As remark, different fits (following different procedures) can lead to slightly different pre-factors c_η – however, the strong fluctuations of the simulation data do not allow for more reliable values. Therefore, we conclude that the error margin of c_η might be as large as 10%. New and better simulations in the future are needed to improve the correction functions and pre-factors.

4.2.5 Energy input rate

Even though the energy input is typically related to the boundary conditions, i.e., to the walls of the system, and not so much to the granular medium itself, we introduce here a temperature/velocity dependent driving mechanism that allows us to specify the energy density input rate J in various ways.

Experimentally, a vibrating wall with different motion modes, like sinusoidal or triangular, is readily realized and the same is true for numerical simulations, see [142–144]. However, the existence of a moving wall makes the formulation of a boundary condition a tricky problem and the overall behavior and dynamics phase dependent. For sake of brevity, we do not discuss this problem here in detail. We only present the non-democratic driving mechanism proposed by Cafiero et al. [145, 146]:

Assume that the system is agitated with a rate $f_{\rm dr}$, ideally with $f_{\rm dr} \gg t_E^{-1}$ in order to decouple the driving from the collision rate. On the other hand, a system vibrating with a given period can be mimicked by setting the driving rate accordingly.

At a driving event at time t, the velocity of a particle i is changed by $\Delta v_i^\beta(t) = r_i^\beta |\mathbf{v}_i(t)|^\delta v_r^{1-\delta}$, where β denotes the independent directions and r_i^β are uncorrelated Gaussian random numbers with zero mean and unit-width. The velocity-change is furthermore proportional to the non-linear power of the absolute velocity $|\mathbf{v}_i(t)|^\delta$ and to a reference velocity v_r that sets the width of the random distribution and scales the non-linear velocity term.

The power δ selects the type of driving with: (i) "democratic" random driving for $\delta = 0$, (ii) "capitalistic" driving for $\delta > 0$, i.e., fast particles gain overproportionally more velocity, and (iii) "communistic" driving for $\delta < 0$, i.e., slower particles gain more velocity. Casting this into a formula, the energy driving term becomes nonlinear in the granular temperature T:

$$J = nH_{\rm dr}T_*^\delta = (\mathcal{D}/2)nf_{\rm dr}T_{\rm dr}T_*^\delta , \qquad (31)$$

with dimensionless $T_* = T/T_r$. For the analytical treatment and plenty of simulations we refer to the literature [145, 146], where also rotational driving is defined [146, 147] with the surprising finding that driving the rotational degree of freedom leads to more homogeneous systems even for very strong dissipation [147].

Note that driving can be applied to the whole system, or locally e.g. at a wall, or with a varying field of $H_{\rm dr}$ as function of the position. Different powers can be chosen to mimic different driving mechanisms, since in nature, not only the random driving occurs. Instead, as an example, it was observed by Cafiero et al. [145], that the power $\delta = 1$ was leading to reasonable qualitative agreement with experiments of a quasi-two dimensional granular gas on a horizontal vibrating table [148] – while $\delta = 0$ did not. Other driving mechanisms might require alternative formulations of J.

The driving method in Eq. (31) also leads to a non-Gaussian velocity distribution, which could be predicted analytically [105, 145, 146]. However, we are not aware that Eq. (31) was ever used in the framework of hydrodynamic equations applied to inhomogeneous situations and used as a (temperature and density dependent) boundary condition.

4.3 Concluding remarks

In this section, various improved forms of the "classical" 2D Enskog "transport coefficients" P, χ, I, κ, and η have been summarized. The starting point was a corrected "global" equation of state, P_Q, with consequently corrected pair-correlation at contact g_Q. The classical g_2 was then replaced by g_Q at every occurrence in the other transport coefficients. For κ and η, further corrections had to be applied in order to bring them in agreement with numerical data from hard sphere ED simulations.

The present results are valid for mono-disperse 2D systems with (rather) weak dissipation and without shear – at all densities. The former three constitutive relations, P, χ, and I, when scaled by their low density limit, just reflect the non-linear behavior of the pair-correlation function that can also be extracted from simulation data straightforwardly by measuring directly either the pressure or the collision rate in a homogeneous (almost) elastic system.

The heat-conductivity κ behaves qualitatively like the pressure but simulations indicate values about 10% larger – without explanation so far. The most interesting transport coefficient is the shear-viscosity, which diverges at a much lower density, ν_η. Thus, this transport coefficient behaves in a qualitatively different way than the others and thus requires a serious correction. Caution is recommended, since the data in Ref. [24] (the only ones known to us) were obtained from an elastic, non-sheared, homogeneous system of mono-disperse hard disks. We are not aware of a direct measurement of κ, but we present a more direct measurement of η below.

5 Special cases

In this section, the complete set of mass-, momentum-, and energy-balance is reduced in complexity by different simplifying assumptions.

5.1 Homogeneous granular gases

When neglecting the mean flux, $u_i = 0$, gravity, $\gamma_i = 0$, and field gradients, $\partial/\partial x_k = 0$, the energy balance equation for a homogeneous granular gas reduces to:

$$\frac{\rho}{2}\frac{\partial}{\partial t}\left(v_T^2\right) = -I + J \ . \tag{32}$$

5.1.1 Homogeneous elastic hard sphere gas

The homogeneous, free, elastic classical gas, $I = J = 0$, conserves energy. Note that the simulation results of the previous section 4 were obtained in this case. Further results involving bi- and polydisperse size distributions and the corresponding collision rates between the different particles were presented in Refs. [75, 116, 117] and will be briefly discussed in subsection 6.7.

Instead of repeating previous results, we present here snapshots of the elastic hard sphere gas at different densities, in Fig. 9, but only show the accumulated centers of the particles as path-lines. From such simulations, the pair-correlation functions and structure-factors can be obtained (data not shown), e.g., see Ref. [116].

For very low density, $\nu = 0.009$, one can see the mean free path, see Eq. (9), $s(\nu)/d = 34.3$, of the particles as line-segments. Already at $\nu = 0.23$, these line-segments become so short, $s(\nu)/d = 0.90$, that they are not visible anymore in this representation. For the higher densities it matters which $g(\nu)$ is used – so we insert g_Q and obtain $s(\nu)/d = 0.096, 0.070, 0.066,$ and 0.059, for increasing ν. Note that the wiggle in g_Q translates to an *increase* of the free path for densities $\nu > 0.67$, relative to the Enskog prediction with g_2. The ordered crystal leaves some more space for the particles to move.

The path-line picture for density $\nu = 0.63$ appears not much different from $\nu = 0.23$. For density $\nu = 0.69$, first traces of the crystallization become visible, and like for $\nu = 0.71$ (not shown), fluid-solid co-existence is evident. For $\nu = 0.73$ as well as for $\nu = 0.75$, the perfect crystal lattice appears. The thickness of the spots indicates the size of the cage they are trapped in. Note that these data were obtained from the idealized case, starting from a perfect lattice.

5.1.2 Driven dissipative hard sphere gas

Driving a granular system homogeneously, using the driving method described in subsection 4.2.5, can lead to a non-equilibrium steady-state (NESS) with mean energy (granular temperature):

$$T^{\text{NESS}} = \left(\frac{\sqrt{2m_0}s_0 H_{\text{dr}}}{(1-r^2)[\nu g(\nu)]T_r^\delta}\right)^{\frac{2}{3-2\delta}} , \tag{33}$$

since the dissipation and energy input cancel each other [105, 146, 149], with fluctuations around this mean. Again the combination $[\nu g(\nu)]$ appears, but this time in the denominator with a δ-dependent power-law. As reported in
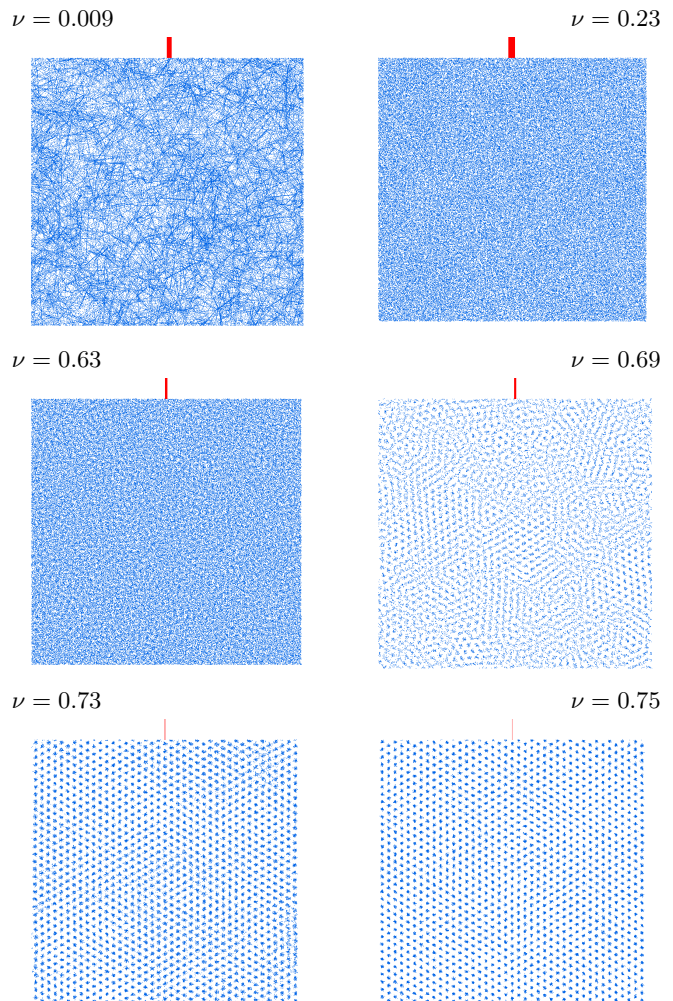
Fig. 9 Path-line snapshots of a periodic, elastic 2D hard sphere system with $N = 1628$ particles at different densities (area fractions ν). Path-lines (blue) are the accumulated positions of the centers of the particles. The red line indicates the fluctuations of the center of mass position in horizontal direction.

Refs. [105, 145, 146], and many other papers since then, e.g., for strong dissipation, the driven granular system is sensitive to instabilities and can develop density fluctuations. This issue is not discussed further in this review.

5.1.3 Freely cooling hard sphere gas

The case $I > J = 0$ corresponds to the freely cooling granular gas. In the homogeneous case, one has the energy density dissipation rate, I, as the only transport coefficient left and can study the effects of crystallization and elasticity at high densities. The homogeneous cooling state (HCS) can be solved analytically, inserting the transport coefficient I from Eq. (11) into Eq. (32):

$$\frac{\rho}{2}\frac{\partial}{\partial t}\left(v_T^2\right) = -\rho\, t_E^{-1}\frac{v_T^2}{4}(1-r^2)\,, \tag{34}$$

with the "Enskog collision rate", see Eq. (7),

$$t_E^{-1}(\nu, v_T) = \frac{8\nu g(\nu) v_T}{\sqrt{2\pi} d} =: \frac{v_T}{s(\nu)} , \qquad (35)$$

leading to:

$$\frac{v_T(t)}{v_T(0)} = \frac{1}{1 + \frac{1}{4}(1 - r^2) t t_E^{-1}(0)} , \qquad (36)$$

where the initial collision rate, $t_E^{-1}(0)$ and the initial velocity occur as scaling constants. If one transforms time to the accumulated number of collisions per particle, $C = t t_E^{-1}$, where the collision rate depends on time itself, the solution reads:

$$\frac{v_T(t)}{v_T(0)} = 1 - \frac{1 - r^2}{4} C , \qquad (37)$$

that is linear in C. Note that the limit $t \to \infty$ corresponds to $C \to 4/(1 - r^2)$ [63, 105].

In the above equations, the equation of state (or the pair-correlation function) are hidden in t_E or C. Since the system is assumed to be homogeneous, these quantities are constants so that the evolution of v_T with time will not be affected when replacing g_2 in Eq. (7) by, for example, g_Q.

For strong dissipation and/or high density, the homogeneous state is instable to perturbations above a certain wave-length and, after an initial homogeneous cooling state, cluster growth can be observed [25, 38, 64, 91, 150], until eventually the cluster size reaches system size. The onset of clustering can be well predicted by hydrodynamic stability analysis. The cluster evolution with time is still an open issue for present research.

Already at the beginning of cluster growth, the assumptions of vanishing flux and gradients are evidently wrong, so that the full set of balance equations has to be considered. After some further evolution of the system, one can observe the co-existence of "vacuum" and "solid" regions, see Fig. 1.

5.2 Simple shear of dissipative hard spheres

In the absence of gravity, $\gamma_i = 0$, and with steady shear flux in x-direction, as well as transformation invariance in y-direction, $u_y = u_z = 0$, $\partial/\partial x = \partial/\partial y = 0$, $u_x = u_x(z)$, and $\partial u_x/\partial z = \dot{\gamma}(z)$, the system is described by:

$$0 = -\frac{\partial \sigma_{iz}(z)}{\partial z} , \qquad (38)$$

for $i = x, y, z$, and

$$0 = -\sigma_{xz}(z)\dot{\gamma}(z) - \frac{\partial q_z(z)}{\partial z} - I(z) . \qquad (39)$$

The energy dissipation is compensated by energy input due to shear heating, so that a steady state is possible with $J = 0$.

In addition to the straightforward steady state solution with $\partial/\partial z = 0$, and

$$\sigma_{xz}\dot{\gamma} = -\eta\dot{\gamma}^2 = -I , \qquad (40)$$

there exist instabilities, like the clustering instability mentioned above in sec. 5.1, see also [51, 68, 100, 103, 151–154], which can lead to shear-banding [52, 54, 131, 155], or even to horizontal heat flux [156], i.e., a higher order phenomenon, possibly related to anisotropy. This anisotropy [10] is special about granular systems not only in vibrated systems [157, 158], but also under shear [77], where a finite first normal stress difference shows up even for low densities [78], and interestingly changes sign when density is increased [73].

Inserting the dissipation rate and shear viscosity from Eqs. (11) into Eq. (40) leads to a (2D) prediction for the the shear stress

$$\sigma_{xz} = -\rho^p \nu^2 g(\nu) \frac{(1 - r^2)}{\sqrt{2}\dot{\gamma} s_0} \left(\frac{T}{m_0}\right)^{3/2} \qquad (41)$$

where some shear rate dependence is hidden in the temperature

$$\frac{T}{m_0} = \frac{\dot{\gamma}^2 s_0^2}{1 - r^2} \left(\frac{1}{G(\nu)^2} + \frac{2}{G(\nu)} + \left(1 + \frac{8}{\pi}\right)\right) \frac{\eta_L}{\eta_Q} , \qquad (42)$$

in a homogeneous sheared system, with the viscosity correction factor η_L/η_Q from Eq. (30).

The prediction in Eq. (42) is compared to numerical simulations, see Fig. 10, of a sheared system with constant volume and $N = 2401$ particles, slowly growing in size in order to scan all densities. The shear rate is $\dot{\gamma} = v_s/L = 10$, with the shear velocity $v_s = 1$ of the upper and lower periodic image and the system size $L = 0.1$. It is evident that neither g_2 nor g_Q alone are able to predict the temperature in the sheared system correctly at higher densities $\nu > 0.5$. The system is heated much more than expected from kinetic theory.

The corrected viscosities η_R, η_K and η_L do predict the onset of divergence much better, even though not quantitatively perfect (the fit K performs best here, but not at low densities due to its third term). All predictions fail at densities $\nu > \nu_\eta$ due to the onset of a shear band (inhomogeneity).

While the shear-band instability and the divergence occur at around $\nu = 0.700 \pm 0.005$ for weak dissipation, for stronger dissipation (data not shown) $r = 0.95$, and 0.90, the shear-band instability occurs at higher densities $\nu = 0.73 \pm 0.01$, and 0.78 ± 0.01, respectively. The occurrence of the shear-band instability can be related to the increased shear stress. Considering the viscosity-divergence, the shear band instability occurs at lower densities due to the increased shear stress and temperature, as was shown in the framework of a linear stability analysis (compare models A without, and C with the

---

[10] *Anisotropy* here either means (i) more collisions in one direction than the other, in dynamic systems, or (ii) more contacts in one direction than the other, for static systems.
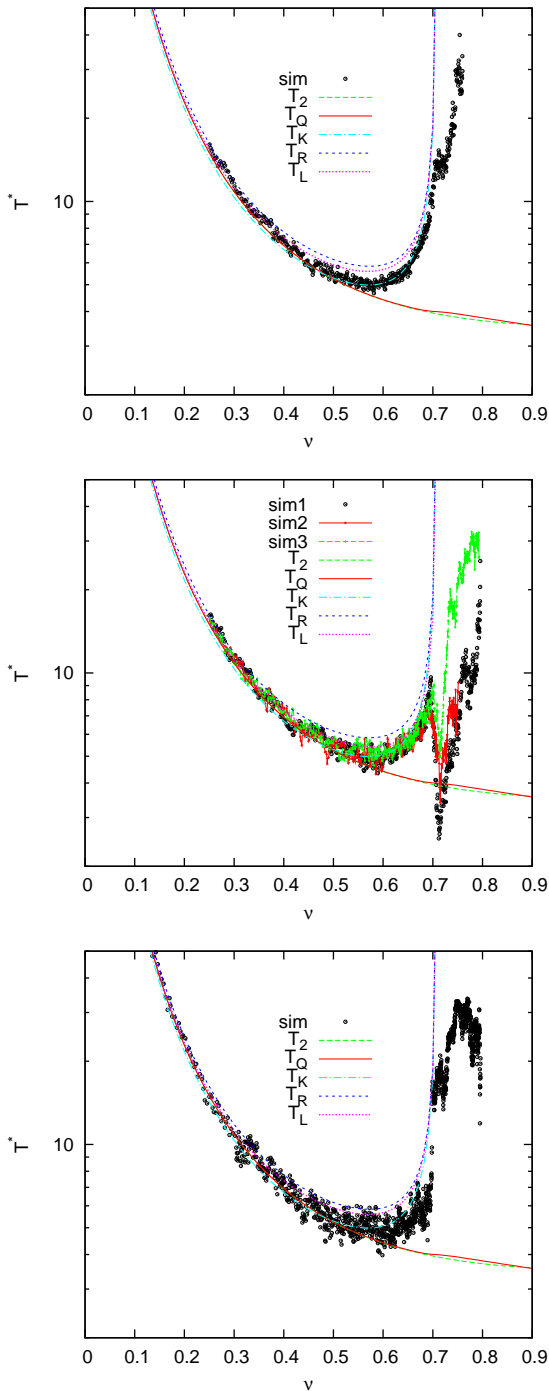
Fig. 10 Scaled temperature $T^* = T(1-r^2)/(m_0\dot{\gamma}^2 s_0^2)$, plotted as function of density from a 2D sheared system (using Lees-Edwards boundary conditions) with $r = 0.998$ (Top), $r = 0.995$ (Mid), and $r = 0.99$ (Bottom). Symbols (points) are simulation data and the various viscosities are denoted as 2 (Enskog), R [24], K [52], and L, Eq. (30), respectively. In the mid-plot, the different colors/symbols represent different initial conditions.

divergence, in Ref. [131]). Note that the system can explore states beyond the divergence of η and T^*, at higher densities $\nu > \nu_\eta$, by bifurcating into a solid part and a shear band with zero and finite shear-rate, respectively, as was examined in Refs. [52, 54, 155]. A more detailed study of this system is in progress.

5.3 Granular gas in gravity – elastic limit

A steady state with $u_i = 0$, translation invariance in x- and y-directions, and gravitational acceleration $g_z = -g$, is described by:

$$\frac{\partial \sigma_{iz}}{\partial z} = 0 \ , \ \text{for} \ \ i = x, y \,, \tag{43}$$

$$\frac{\partial \sigma_{zz}(z)}{\partial z} = -\rho g \,, \tag{44}$$

and

$$\frac{\partial q_z(z)}{\partial z} = -I(z) + J(z) \,. \tag{45}$$

These equations are valid for 2D and 3D, where, in the former case, the y-direction is dropped.

In a vibrated system, if the energy input is located at the bottom, z_0, of the system, the source term J forms a boundary condition rather than a bulk transport coefficient. Alternatively, one can apply homogeneous driving [124] or other variations of energy input. However, in the following, we mostly focus on the 2D elastic case.

5.3.1 Elastic limit in 2D

In the elastic limit without energy input, T is constant even when the wall is fixed, and only the ordinary differential equation (44) remains, which allows us to study the pressure, p, in detail for all densities [45, 115, 116].

Assuming an isotropic elastic hard sphere gas in gravity, one has $p = \sigma_{zz}$ and thus:

$$\frac{dp(z)}{dz} = -nm_0 g \,. \tag{46}$$

After multiplication with the particle volume, $V^{(p)}$, one can replace n by ν leading to: $pV^{(p)} = \nu T(1 + 2\nu g_\alpha(\nu))$, so that:

$$\frac{d(pV^{(p)}/T)}{d\nu} = \left(1 + 4\nu g_\alpha(\nu) + 2\nu^2 \frac{dg_\alpha(\nu)}{d\nu} \right) \tag{47}$$

is an analytically known function of ν only. The resulting non-dimensional differential equation

$$\frac{d\nu}{dz'} = -\nu \left[\frac{d(pV^{(p)}/T)}{d\nu} \right]^{-1} \,, \tag{48}$$

can be solved (numerically), for the different g_α, with scaled height $z' = z/z_T$ and $z_T = m_0 g/T$.

The solution, i.e., the density ν is plotted against the scaled height z/z_T for different numbers of particles N, see Fig. 11.

From

$$N = \frac{A}{V^{(p)}} \int_0^\infty \nu(z)dz \,, \tag{49}$$

from which we obtain the filling height at maximal density: $z_N = NV^{(p)}/(A\nu_m)$, and the filling factor:

$$\nu_m \frac{z_N}{z_T} = \frac{NV^{(p)}}{z_T A} = \int_0^\infty \nu(z')dz' \,, \tag{50}$$

as used as a parameter in Fig. 11. The profiles for different equations of state α are plotted as indicated in the inset.
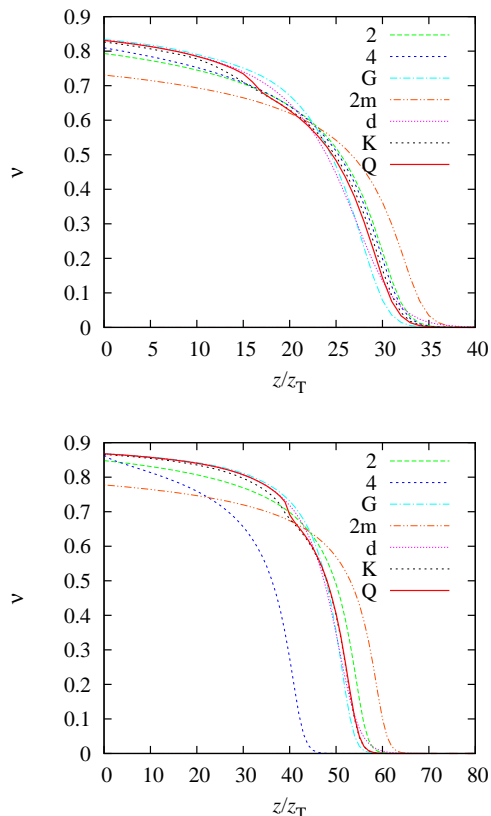
Fig. 11 (Color online) 2D density as function of dimensionless height z/z_T for different $g_\alpha(\nu)$ with α given in the inset. The filling factors are $\nu_m z_N/z_T = 20$ (Top) and 40 (Bottom). The blue line in the bottom plot does not fulfill the integral boundary condition, since g_4 fails at high densities.

Looking from the distance most curves seem to agree, at least qualitatively. However, looking more closely, we observe that the form g_{2m} fails mostly – it even leads to a different exponential tail (details not shown). The form g_1 fails already for small filling heights and is therefore not shown. The function g_4 deteriorates for $\nu > 0.78$ and

thus should not be used. The other forms are similar and agree within about 5-15%. Using either g_K or g_Q leads to similar density profiles, only for g_Q the density drop at $\nu \approx 0.70$ is much more pronounced.

5.3.2 Towards weak dissipation

A few simulations with weak dissipation and weak energy input show qualitatively the same density profile as in the elastic limit (data not shown). However, a more systematic study of the inelastic granular gas, beyond the first results by Carrillo et al. [56] – with the goal to evaluate the different constitutive relations – is still to be performed.

5.3.3 Conclusion

In conclusion, if one wants to decide what is the form of g_α that leads to best agreement with a simulation or an experiment, one should examine the data very closely. An error-level much below 10% is needed. The pair correlation function g_Q was shown to agree best with numerical simulations and experiments in [115, 116], however, g_K with a smoother transition zone at $\nu \approx 0.7$ also performs reasonably well. To our knowledge, there exist only few experimental data [110, 111], which could allow us to distinguish which of the two alternatives performs better. The question about the systematic deviations between real experiments and the idealized hard sphere system remains open.

5.4 Other special cases

In this section, some special cases – particularly simple ones – were discussed. These situations should be examined more closely by new, careful experiments in order to judge the validity and relevance of the corrected pair correlation function. Also the corrections to the constitutive relations for the other transport coefficients require a closer look at density- and temperature-profiles.

Other special cases like, e.g., flow on an inclined plane were examined in detail already numerically and theoretically [17, 29, 33, 50, 58, 103, 159, 160]. The corrections proposed in this study – applied to the inclined plane boundary condition – are expected to show the co-existence of static (dense, no-shear) and dynamic (shear) layers due to the viscosity term that diverges at a density lower than the maximum density. However, this will be studied elsewhere.

6 Towards more realistic models

This section is dedicated to the discussion of realistic granular material properties. Which quantities and properties are important in realistic situations and how can

the equations of state (transport coefficients) be modified in order to account for them?

In the following subsection 6.1, first a general review will be given, before the issues of elasticity and multi-particle contacts are addressed in subsection 6.2. The effects of stronger dissipation and friction are discussed in subsection 6.3 and 6.4, respectively, before long range forces and wet granular media are briefly addressed in subsections 6.5 and 6.6. Finally, particle size distributions other than mono-disperse (e.g., bi- and polydisperse) are discussed in subsection 6.7 and the effect of different shapes is briefly pointed out in subsection 6.8. The extension of the present 2D results towards 3D systems is discussed in section 6.9.

6.1 Overview of recent research

In the review paper by Hutter [161], various models are introduced to describe, e.g., relatively shallow flows on inclined surfaces. Other situations involve more dynamics [32], quasi-static flow [34, 162] or wet contacts [26, 31]. Also structure formation [25, 30] and non-standard rheology in dense flows [33, 50, 53] as well as various types of instabilities in complex fluids [154, 163] were reviewed. In general, granular systems show the co-existence of dense, static and more dilute, dynamic regions [27–29, 58]. The greatest challenge is to describe this co-existence in the framework of a hydrodynamic theory, see the previous sections 4 and 5.

The dilute and moderately dense limit is described well by kinetic theory, and the previous sections show that also the dense, almost elastic limit can be described when using the global equations of state, i.e., corrected constitutive relations that are valid for all densities. However, in many systems additional effects can come into play and, e.g., higher dissipation or friction has to be taken into account. For results on advanced kinetic theory in the presence of (possibly strong) dissipation, see Refs. [35, 66, 68, 164], and for measuring transport coefficients using the Green-Kubo relations, see e.g. Refs. [35, 165] and references therein. Observations in ideal systems already involve non-Maxwellian velocity distributions [146], correlated velocities [166] and hydrodynamic instabilities that can lead to structure formation [25, 30, 38, 46] and non-standard rheology in dense flows [29, 50, 53, 58]. Various types of instabilities in complex fluids are reviewed, e.g., in Refs. [35, 36, 154, 163] and references therein.

In the next subsection, elasticity of particles is discussed as the first example of non-classical phenomenology.

6.2 Elasticity and multi-particle collisions

Idealized granular systems are described qualitatively in the original paper by Haff [2] – a work that was followed by many, more quantitative studies using the mighty framework of kinetic theory [66, 96, 97, 101, 102, 107, 165, 167–171]. A generalization of Haff's work towards soft particles (the only known to us) was attempted by Hwang and Hutter [172], who included the finite contact duration into the model. While rigid spheres imply instantaneous collisions, and kinetic theory assumes binary collisions only, in realistic systems with soft particles, multi-particle contacts are possible.

A theory that describes the behavior of rigid particles is the kinetic theory [66, 173, 174], where collisions take place in zero time (they are instantaneous), exactly like in the hard-sphere model. Multi-body interaction can be accounted for via an extension to higher order correlations [63, 105, 174]. However, this does not account for elasticity. During a contact, *potential energy* is stored (reversibly and thus elastically). This *elasticity* effect is also related to the so-called "detachment-effect" [175, 176]: Collisions that take a finite time, during which a part of the energy, i.e., the elastic, potential energy fraction, is not dissipated. Thus, frictionless particles with multiple contacts behave more elastic than a binary collision model would predict. Multi-particle contacts dissipate less energy, as can be shown by comparing soft-particle with rigid particle simulations [46].

Multi-particle interactions [46, 75], and a thus reduced dissipation at higher densities [42, 75], were proposed as a phenomenological model in order to take into account the non-zero contact duration t_c. Due to the commonly used symbol, t_c, the model is referred to as the TC-model, as specified below. Also the radial distribution function at high density has been recently revisited and enduring contacts and their "age" have been studied [177] (for different contact models) as well as the related stress relaxation under shear. Multi-particle contacts and elasticity were reported to affect the rheology of flow on inclined planes, see e.g. Refs. [33, 178, 179].

6.2.1 Elasticity and contact duration

The elasticity and the related finite contact duration can be used to modify all transport coefficients. Hwang and Hutter [172] extended the work of Haff [2] to describe higher densities and, in addition, introduced the notion of a "contact duration" into the theory. They define the time of encounter $t_e = t_f + t_c$ with the time of free flight t_f and the contact duration t_c. The limit of $t_c \to 0$ leads to the definitions of Haff, where $t_f \approx t_E \propto s/v_T$ is proportional to the ratio of the typical separation s and the typical fluctuating velocity v_T, see Eq. (7).

For $t_c = 0$, the collision rate is t_E^{-1}, diverging for $s \to 0$. For $t_c > 0$ the number of collisions per particle per unit time is estimated by $f_c \approx t_e^{-1}$. A finite maximal collision frequency is obtained for vanishing s, so that $t_e^{-1} \to t_c^{-1}$ for increasing density $s \to 0$. Therefore, the generalized collision frequency t_e is bounded by a finite maximum so that an artificial effect like the "inelastic

collapse" [38,40], i.e. the divergence of f_c, cannot occur. Unfortunately, the ideas proposed in Ref. [172] are qualitative so far; it is not clear (and has not yet been shown to our knowledge) how to extend kinetic theory towards non-zero t_c values in this framework. All transport coefficients will be affected by a finite $t_c > 0$, however, in the following only the modification of the energy density dissipation rate will be discussed, since we believe it is the most important modification needed.

6.2.2 TC-model

For hard spheres, the typical time between encounters, $t_e = t_f = s/v_T$ cannot be modified [180, 181], since $t_c = 0$. However, in the framework of the TC model, one can distinguish between dissipative and elastic collisions. Given the time $t_n^{(i)}$ that passes by between collision $n-1$ and n of particle i, the coefficient of restitution for collision n can be expressed as

$$r_n^{(i)} = \begin{cases} r & \text{for } t_n^{(i)} > t_c \\ 1 & \text{for } t_n^{(i)} \le t_c , \end{cases} \tag{51}$$

with $0 < r \le 1$. Thus the type of a collision changes from inelastic to elastic when collisions occur too frequently. More specific, a collision is elastic if *at least one partner* fulfills the above condition $t_n^{(i)} \le t_c$. If t_c and r depend also on the relative velocity [175, 176, 182], the material behavior could be adjusted using this dependence, however, we do not attempt this here.

Even though using the memory of a previous collision does not correspond to true multi-particle collisions, the elastic collisions are denoted as multi-particle collisions [42, 75]. The particles involved contribute to the (elastic) potential energy of the system. The total energy is thus not changed, only part of it is denoted as "potential energy" – i.e. the kinetic energy related to rapid collisions. The potential energy is not dissipated while the remaining kinetic energy is.

6.2.3 The TC model correction to the dissipation rate

The TC-model was applied to freely cooling systems in 2D [42] and 3D [75]. In the homogeneous cooling state (HCS), the conservation equations reduce to an ordinary differential equation, as shown in subsection 5.1.3.

In the framework of the TC model, the energy dissipation rate must be extended by an exponential correction factor:

$$I_c := I(t_c) = I_\alpha \exp\left(\Psi(\tau_c)\right) , \tag{52}$$

with I_α from Eq. (10), where $g = g_\alpha$. The collision rate in I_α is denoted as t_α^{-1} and allows us to define the dimensionless (Luding) number [42]:

$$\tau_c = \frac{t_c}{t_\alpha} , \tag{53}$$

which is $\tau_c = 0$ for the classical hard sphere gas with $t_c = 0$ and $\tau_c > 0$ for finite contact duration in realistic systems. [11] The contact duration t_c has no effect when the time between collisions is very large $t_\alpha \gg t_c$, but strongly reduces dissipation when the collisions occur with high frequency $t_\alpha^{-1} \gtrsim t_c^{-1}$.

In 2D, the variable of the exponential correction term is $\Psi_{\text{LM}}^{2D} = -2\tau_c$, as proposed by Luding and McNamara [42], based on probabilistic mean-field arguments. Their numerical simulations indicate that a correction factor of the order of 0.95 might be appropriate (in 2D), but we are not aware of a more detailed numerical or theoretical study that supports this empirical observation.

In 3D, the correction term argument reads

$$\Psi_{\text{LG}}^{3D} = c_1\,x + c_2\,x^2 + c_3\,x^3 + \mathcal{O}(x^4) \tag{54}$$

with the dimensionless argument $x = \sqrt{\pi}\tau_c$, as obtained from kinetic theory [75], and the constants $c_1 = -1.268$, $c_2 = 0.01682$, and $c_3 = -0.0005783$. Note that the first term yields $\Psi_{\text{LG}}^{3D} \approx -1.9972\,\tau_c$, which is almost identical to the 2D correction term.

6.2.4 Free cooling 3D gas with elasticity $\tau_c > 0$

The differential equation (34) describes the HCS of a freely cooling granular gas at moderate densities, and can be corrected by the exponential term in Eq. (52)

$$\frac{\rho}{2} \frac{\partial}{\partial t} \left(v_T^2\right) = -I_c = -I \exp(\Psi) \approx -I \exp(-2\tau_c), \tag{55}$$

where the rightmost term is valid for 2D and 3D approximately (within a few per-cent for $\tau_c < 1$). Eq. (55) is solved numerically and compared to simulation results – both data sets are scaled by the classical solution $E_2(\tau)/E(0) = 1/(1 + \tau)^2$, for $\tau_c = 0$ in Fig. 12 (Top). The agreement between 3D simulations and 3D theory is almost perfect in the examined range of t_c-values, only when deviations from homogeneity are evidenced one observes disagreement between simulation and theory.

Thus, in the homogeneous cooling state, given that τ_c is sufficiently large, there is a strong effect initially. However, the long-time behavior tends towards the classical decay $v_T^2 \propto t^{-2}$, since the correction term tends towards unity for t_E^{-1} decaying with time.

The ultimate check whether the ED results for soft, elastic systems (which have finite t_c and a potential energy during contact) modeled by the TC model are reasonable, is to compare them to soft-particle MD simulations, also referred to as DEM (Discrete Element Method), see Fig. 12 (Bottom) Ref. [46] for details, and [29] for another example. Open and solid symbols correspond to soft and hard sphere simulations, respectively. The qualitative behavior (the deviation from the classical HCS

---

[11] Note that in Ref. [42] the inverse definition was used. However, here we adopt the definition of the later publication Ref. [75], since with this definition $\tau_c \to 0$ is a small dimensionless quantity for $t_c \to 0$, i.e., in the classical hard sphere limit.
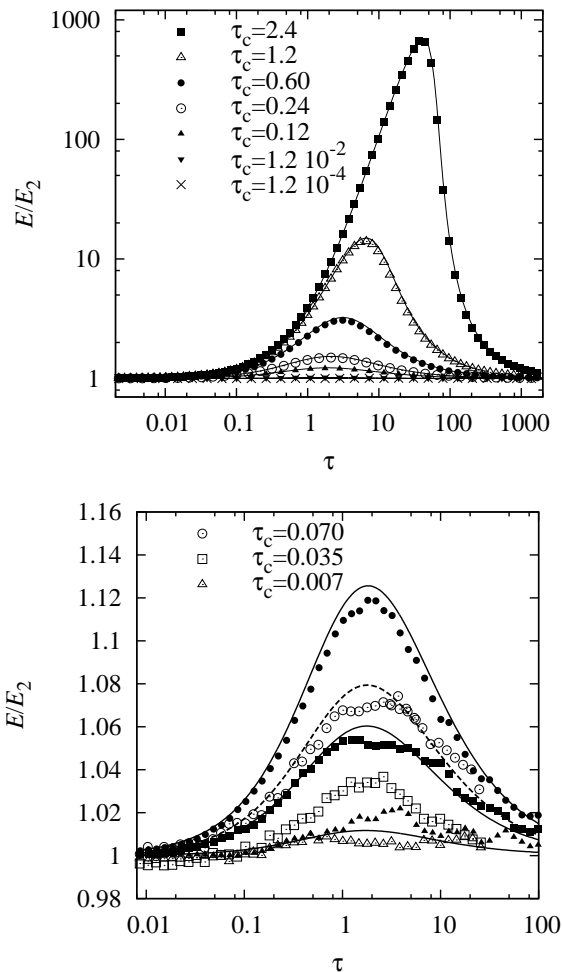
Fig. 12 (Top) Deviation due to finite contact duration, t_c, from the HCS in 3D, i.e. rescaled energy E/E_2 [75] plotted against scaled time $\tau = \frac{1}{6}(1-r^2)t/t_E(0)$, for simulations with different initial $\tau_c(0) = t_c/t_E(0)$, as given in the inset, with $r = 0.99$, $\nu = 0.1134$, and $N = 8000$. Symbols are ED simulation results and the solid line results from the third order correction Eq. (54). (Bottom) E/E_2 plotted against time τ for simulations with $r = 0.99$, $\nu = 0.0736$, and $N = 2197$. Solid symbols are ED simulations, open symbols are MD (soft particle simulations) with three different τ_c as given in the inset. The solid line represent the corresponding analytical solutions – matching the ED data – while the dashed line involves the correction factor $\beta_c = 0.65$ – matching the MD data.

solution) is identical: The energy decay is delayed due to multi-particle collisions, but later, after the systems is considerably cooled down, the classical solution is recovered.

A more quantitative comparison shows that the deviation of energy from the classical solution is larger for ED than for MD, given that the same t_c is used. (Rather small τ_c are used here, since larger τ_c corresponds to much softer particles for which considerable overlaps are found.)

The reduced dissipation was first observed in MD simulations [175, 176]. It can be understood from the above arguments – for ED, the strict rule used for reducing dissipation is under-predicting the energy loss: Dissipation is inactive if any particle had a contact some short time ago. In MD – and in reality – the reduction of dissipation is continuously increasing during the collision until maximal deformation, and then continuously decreasing again. The disagreement between ED and MD is systematically increasing with increasing contact duration t_c (data not shown) and can be corrected if a smaller t_c value is used for ED, so that $t_c^{\mathrm{ED}} \approx \beta_c\, t_c^{\mathrm{MD}}$, with $\beta_c < 1$ (e.g., for the simulation with $\tau_c = 0.07$, a value of $\beta_c = 0.6$ provides an analytical solution close to the MD results (dashed line). However, no further quantitative study is known to us that would provide a theoretical foundation to this observation.

The disagreement is plausible, since the TC model disregards all dissipation for multi-particle contacts, while the soft particles still dissipate energy - even though much less - in the case of multi-particle contacts [175].

6.2.5 Shear flow

The TC model was rarely applied to shear flow situations. For more details on dense shear flow theory, see Ref. [183] and references therein. The most recent results, to our knowledge, involve shear bands with dilute zones with high shear-rate and static, solid-like plugs without internal shear [52, 54, 100, 103], but no effect of elasticity. Different equations of state at different densities and dissipation strengths were examined [131], but no systematic study of the elasticity was performed yet, to our knowledge.

6.3 Stronger dissipation

Throughout this review, the almost elastic limit, $r \to 1$, was considered for sake of brevity. Even though many simulations were performed for perfectly elastic particles, a few tests with weak dissipation indicate that the statements made in this paper also hold for weak dissipation. For a more quantitative study of different values of r, see e.g. subsection 5.2, where especially the divergence of η at small densities is verified for dissipation with $r \geq 0.99$.

The kinetic theory for disks with considerable dissipation [36, 77, 97, 102, 184, 185] leads to transport coefficients with r-dependent factors, see e.g. Ref. [36, 100, 102, 103] and references therein for more details. Here, only the results of Ref. [102] are revisited, which do contain r-dependent terms, but neglect higher order gradients/moments and corrections to the distribution functions [36, 101]. Anisotropy and other effects [77, 96] should not be expected in this level of approximation. For $r < 1$,

but not too small, according to [100, 102, 103, 186], the transport coefficients from Eq. (10) are:

$$p = \frac{\rho^p \nu\, v_T^2}{2}\left(1 + 2G\right)\,, \tag{56}$$

$$\eta = \frac{\rho^p \nu\, v_T s_0}{2G}\left\{\frac{2(1+r)}{7-3r} + \frac{(3r+1)(1+r)}{(7-3r)}G \right.$$
$$\left. + \left(\frac{(1+r)(3r-1)}{(7-3r)} + \frac{8}{\pi}\right)G^2\right\}\,,$$

$$\chi = \rho^p \nu v_T s_0 \frac{8}{\pi}G\,,$$

$$\kappa = \frac{2\rho^p \nu\, v_T s_0}{m_0 G}\left\{\frac{4}{19-15r} + 3\frac{2r^2 + r + 1}{19-15r}G \right.$$
$$\left. + \left(\frac{9(1+r)^2(2r-1)}{4(19-15r)} + \frac{4}{\pi}\right)G^2\right\}\,,$$

$$I = \frac{\rho^p \nu G v_T^3}{2s_0}(1-r)\left[1 - \frac{3s_0}{v_T}\frac{\partial u_k}{\partial x_k}\right]\,,$$

$$\lambda = -m_0 s_0 v_T^3 \frac{3r(1-r)}{19-15r}\left(1 + \frac{3}{2}G\right)\left(1 + \frac{\nu}{G}\frac{dG}{d\nu}\right)\,,$$

rewritten such that the object

$$G := G(r,\nu) = \frac{1}{2}(1+r)\nu g(\nu)$$

occurs, instead of the $G(\nu) = G(r = 1, \nu) = \nu g(\nu)$. With this it is possible to use the G_α (with the corresponding g_α) together with considerable dissipation. Note that the (second and higher) Sonine coefficients (a_2, ...) are neglected above for the sake of brevity. The expressions for these terms, in the low density limit, can be found in Refs. [36, 99, 185], while expressions for 3D and moderate densities can be found, e.g., in Refs. [101, 170]. For even more elaborate transport coefficients for small $r \ll 1$, mostly in the low density limit, in 2D and 3D, see, e.g., Ref. [36, 66, 96, 101, 170, 187] and references therein. Discussing strong dissipation in the extreme case of completely inelastic collisions $r = 0$, see for example Refs. [188, 189], is far from the scope of this paper.

6.4 Friction

Friction leads to a coupling of rotational and translational degrees of freedom [190–194] and (due to dissipation) to non-equipartition of energies [142, 143, 157, 158, 195], and correlations between the different degrees of freedom [166]. The presence of friction and the rotational degrees of freedom has been related to a random restitution coefficient [196, 197], however, we disregard here this stochastic approach to a deterministic problem.

Only for nearly smooth or perfectly rough particles, the system evolution and transport coefficients can be computed analytically [198–200]. In the intermediate range of realistic friction coefficients, $0.1 \leq \mu \leq 1.0$ rather involved implicit integral equations have to be solved numerically [193]. The latter allow for asymptotic analysis that manifest the reference situations at which simplified models can be tested.

For perfectly rough particles, a constant tangential coefficient of restitution, r_t, is used. For slightly frictional, almost smooth particles, the translational and rotational degrees of freedom can decouple and thus behave singularly, i.e. one of the energies decays rapidly, whereas the other remains almost constant.

For intermediate values of friction, the use of a renormalized, effective coefficient of restitution was proposed [201] as:

$$r_{\text{eff}} = r - \mu + 2\mu^2(1+r)\,, \tag{57}$$

however, to our knowledge, without quantitative validation so far. As an application, the hydrodynamic equations with the transport coefficients for smooth particles can be used together with this effective coefficient of restitution for the description of non-uniform shear flows [100]. The more advanced theory involves also the rotational energy [102] and was applied to shear flow on a bumpy boundary [103] *not* using the effective restitution, but the constant tangential restitution collision model. Note however that an effective normal restitution ignores the fact of energy non-equipartition. This is fatal, since already in homogeneous (cooling and driven) systems [193], the energy dissipation and transfer terms for translational and rotational degrees of freedom depend on the ratio of rotational and translational temperature.

In order to predict the evolution of the temperatures R and T for homogeneously cooling systems without shear, the most realistic Coulomb friction model [202] was used, involving sliding and sticking contacts [193]. The involved kinetic theory, which leads to almost perfect agreement with simulations [193], was solved assuming Maxwell distributions for both translational and rotational velocities. The comparison with theory shows that a full representation of friction has quantitative predictive value [193, 203] for intermediate coefficients of friction. Several simplified models for friction show qualitative agreement, however, quantitatively there is no effective tangential restitution reported to our knowledge (and thus no effective normal restitution) that could be used for realistic systems. The full set of kinetic theory integrals has to be solved in order to properly account for Coulomb-type friction.

Note that the presence of friction and other forces, as introduced in the following, can lead to a change of important properties. For example, with increasing friction, one expects that the maximal packing density ν_m decreases. However, the issue of the material dependent packing density and related effects like jamming is far beyond the scope of this review.

6.5 Long-range forces

When repulsive or attracting long-range forces act in addition to the hard-core repulsion and dissipation in a granular gas, the behavior becomes much more complicated.

Repulsive systems, in general, reduce the collision rate and thus the energy dissipation rate (but not necessarily the pressure – since momentum exchange also takes place without/before contact). Attractive systems, on the other hand, enhance collisions, since particles have more difficulty to separate.

In the limit of zero density and rather weak long-range forces, a Boltzmann-like correction factor to the energy dissipation rate was determined using kinetic theory arguments for the energy dissipation rate. For repulsive systems [204–207]:

$$I_{\rm rep} = I_\alpha \exp\left(-\frac{E_b}{T}\right) \tag{58}$$

and for attracting systems [206, 207]:

$$I_{\rm atr} = I_\alpha \left[2 - \exp\left(-\frac{E_e}{T}\right)\right] , \tag{59}$$

with I_α from Eq. (10).

In Eq. (58), the energy E_b corresponds to the *energy barrier*, two particles have to overcome before they can collide, when approaching from infinity. In Eq. (59), the energy E_e corresponds to the *escape energy* two particles have to overcome after a collision, so that they can separate.

Already for small densities, multi-particle effects and correlations disturb the simple and straightforward corrections above. An effective energy $E_{b,e}^{\rm eff} = \alpha(\nu)E_{b,e}$ was proposed by Müller [206], where the empirical correction term $\alpha(\nu)$ (obtained from numerical particle simulations) decays exponentially fast with density and is rather small already for densities $\nu > 0.4$. This means that, interestingly, the long-range effect, as described by the corrected I above, becomes weaker for higher densities.

In the moment we are neither aware of an analytical prediction for this multi-particle behavior nor of simulation results at higher density granular systems in the presence of strong long-range forces.

6.6 Wet Granular Media

In Ref. [31], an expression for the near-contact pair correlation function of $\mathcal{D}$-dimensional weakly polydisperse hard spheres is presented, which arises from elementary free-volume arguments. When the particles are wetted, they interact by the formation and rupture of liquid capillary bridges.

During the (hysteretic) interaction, a typical energy $E_{\rm cb}$, is lost and the system behaves "sticky" when $E_{\rm cb} \gg$ T. This finally yields an analytic expression for the equation of state, P, of wet granular matter for $\mathcal{D} = 2$, valid in the complete density range from gas to jamming. For $E_{\rm cb} \ll T$ the system behaves almost as described in this review, while for "sticky" systems, new features and instable regimes occur in the equation of state.

Since all this is described in detail in the studies by Mitarai and Nori [26] and by Fingerle and Herminghaus [31, 208], we do not provide detail here. We only remark that, again, the correction to the "classical" system involves the ratio of two energies $E_{\rm cb}/T$, like for long-range forces, see subsection 6.5.

6.7 Particle size-distributions

Realistic materials consist of particles of different size. Bi-disperse (binary) size distributions are often used in experiments to avoid crystallization. The transport coefficients for binary mixtures are known, see e.g. [75, 95, 115, 116, 130, 209–213] and references therein, and have recently been improved using a self-consistent formulation involving also g_Q instead of g_2, see Ref. [117]. This way, the validity of the pair correlation functions can be extended to higher densities They can be used to predict mixing and segregation of two species [124, 214–218].

However, realistic granular materials come with a polydisperse size-distribution with particular shape like, e.g., log-normal distributions. While wide size distributions are not discussed in this study, rather narrow and homogeneous polydisperse size-distributions were studied, e.g., in references [75, 115, 118, 119, 213, 219–223].

In our opinion, the most note-able attempt to unify the description of bi- and poly-disperse size distributions was proposed in 2001 [115] and further studied later [75, 117]. The classical pair-correlation functions for two species [95] are expressed as functions of the size-ratio and the number-fraction. Rewriting the same formulas in terms of the moments of the size-distribution as

$$g_{\mathcal{A}}(\nu) = \frac{1 + \mathcal{A} - \nu(1 - \mathcal{A}/8)}{2(1 - \nu)^2} , \tag{60}$$

with the non-dimensional width of the size-distribution $\mathcal{A} = \langle a \rangle^2 / \langle a^2 \rangle$, eliminates one parameter and allows us to predict the non-dimensional collisional pressure,

$$P(\nu) = (1 + r)\nu g_{\mathcal{A}}(\nu)\left[1 - a_g \nu^4\right] , \tag{61}$$

with $a_g \approx 0.1$, valid for $\nu < 0.65$, see Ref. [115]. Remarkably, the same expression holds also for poly-disperse particle size distributions, as tested in Ref. [75] (as long as the distributions are not too wide).

For higher densities, like in the mono-disperse case, excluded volume effects lead to an increased pressure with a divergence at $\nu_m < 1$. For bi- and poly-disperse systems, ν_m is a function of the composition of the mixture [75, 112, 115], but we are not aware of a prediction of

its functional behavior, even though extensive numerical simulations are available in the literature.

The pair-correlation function and the equation of state can be constructed in the same spirit as for the monodisperse case. The theoretical prediction for low and moderate densities is merged with an empirical high-density expression [112,115]. The "classical" equation of Torquato [110–112] does not contain a size-distribution parameter, while the expression of Luding [115] in Eq. (60) does. Both expressions have in common with the monodisperse case that they diverge at ν_m, which is an unknown function of the size distribution, in general. However, for disordered systems, the fluid- and the solid-branch seem to merge rather smoothly – without an indication of the crystallization as evidenced in the monodisperse case.

6.8 Various particle shapes

Concerning non-spherical particles, the amount of literature is rapidly growing. Concerning rigid non-spherical particles, we provide the studies of Donev et al. [224–227] as a mere starting point for further literature search.

Concerning soft non-spherical particles, we refer to the well-cited classical works by Schinner et al. [228] and Kun et al. [229] for 2D polygons. More recent studies [230, 231] for 3D non-spherical objects at high densities involve effects like packing and crystallization (e.g. of spherocylinders), or jamming for ellipses [232, 233], just as some examples.

Further discussion of non-spherical objects goes beyond the scope of this review.

6.9 Towards 3D

A one-dimensional system is artificial in the sense that particles cannot pass-by each other. But most observations and statements in this paper are expected to be valid in both 2D and 3D systems. The data presented in this study were mainly 2D, with a few 3D situations and examples.

While the phenomenology, i.e., the co-existence of dilute and dense regimes as well as the existence of dissipation and friction, is independent of the dimension, the balance equations of mass, momentum and energy are slightly different in the pre-factors of the constitutive relations, but not in the shape of the equations: The 3D transport coefficients have different pre-factors, as compared to those reported for the 2D situation in this review.

For sheared systems in 3D, just to give some examples, the density correlations were recently examined in detail [155], also with soft spheres [132]. One difference to the data presented in this study manifests in 3D: The viscosity divergence density, ν_η, seems to be related to

the crystallization density, ν_c, and moves towards higher densities with increasing dissipation or when different sized particles avoid crystallization. In 3D crystallization is much less favorable than in 2D and thus the viscosity divergence has to be examined more closely in 3D:

Is the divergence at $\nu_\eta < \nu_m$ an artefact of the monodisperse system and 2D, or can it also be found in more realistic, disordered systems in 3D?

Another qualitative difference between 2D and 3D is the fact that crystallization under slow volume-change in 2D does not show much hysteresis, whereas the hysteresis in 3D is much stronger, as studied in detail, e.g., by Donev et al. [27].

Here we present data from 3D hard sphere simulations, where the particle radii are growing with specified rates, see Fig. 13 (Top), and shrinking with the corresponding rates, see Fig. 13 (Bottom). Changing the growth-rate over several orders of magnitude (see inset), we observe a rate-dependent over- or under-pressure for growing and shrinking particles, respectively. Growing leads to additional collisions, while shrinking leads to reduced collisions.

The ordering/crystallization in 3D occurs at a higher density than the melting transition. These transition densities also depend on the rate of change of density. For very slow changes (10^{-7}) the situation is almost quasi-static and rate-independent, but still shows a considerable hysteresis cycle. Then the transition is rather sharp for increasing density and quite smooth for decreasing density. For the fastest changes, the crystallization/melting transition mutually disappears and only the over- and under-pressure can be observed.

A global equation of state was not yet proposed in 3D systems due to the hysteresis during crystallization and melting. We are not aware of a theoretical model that describes this regime. For low and high densities, the kinetic theory and free-volume models, respectively, work in 3D as well as in 2D. This renders the (hysteretic) crystallization/melting regime as a challenge, if one wants to proceed with 3D models in the same spirit as proposed in this paper for 2D.

Finally, we remark that there also exist "2.5-dimensional" systems [55, 57] where the (experimental laboratory) system is short in one direction and long in the two others. Due to the presence of walls, the equations of state (and other details) will be different from both 2D and 3D situations (data not shown).

7 Summary

As an example for a simple, representative granular system, the exemplary case of the transition from homogeneous to inhomogeneous cooling and cluster growth was introduced in section 2. This example illustrates the fact that, in granular media, the dilute gas-like regime typically co-exists with much denser fluid-like or even solid
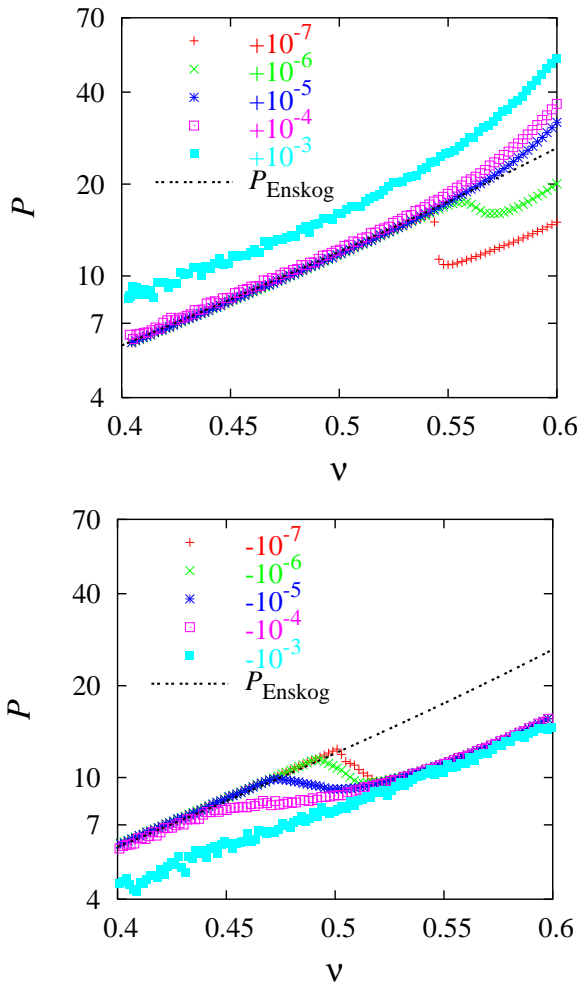
Fig. 13 (Top) Non-dimensional 2D pressure $P = pV/E - 1$ as function of density for different growth rates as indicated in the inset. (Bottom) the corresponding data for different shrinking rates. Simulations are 3D event driven with $N = 2000$ particles and elastic collisions, $r = 1$.

areas, where the density can become extremely high, approaching the maximal possible density.

After the hydrodynamic equations were introduced in section 3, corrections to the constitutive relations for the equation of state and the transport coefficients are provided in section 4, which are then valid for all densities. These make it possible to take into account the different physics when low and high densities occur in the same system at the same time.

The starting points were the kinetic theory prediction for pressure for low and moderate density and a free-volume model for very high densities. From event-driven computer simulations, the transition (crystallization/melting) regime between the fluid/gas and the solid-like state was obtained. This "global equation of state" takes into account the crystallization/melting transition

in 2D (it represents a "smooth Maxwell construction") and improves the predictive value of the model so that it can be applied for all densities.

Other transport coefficients are also corrected using the pair-correlation function – as obtained from collision-rate or pressure. Notably, the heat-conductivity seems to show some small systematic deviation from the theoretical predictions, whereas viscosity shows an unexpected, strong qualitative difference: Viscosity diverges at a density ν_η, much lower than pressure, which diverges at ν_m – at least for mono-disperse, 2D systems as mostly studied here. Special (simplified) cases of the hydrodynamic equations were reviewed in section 5 and some examples were given supporting the earlier observations on a divergent viscosity at low densities, close to the crystallization/melting density. *The question how these observations are related to the concept of jamming is not discussed in this review.*

In section 6 further corrections towards more realistic systems involve:
(i) multi-particle interactions and elasticity
(ii) strong dissipation,
(iii) friction,
(iv) long-range forces and wet contacts
(v) wide particle size-distributions, and
(vi) various particle shapes.
These corrections allow the use of kinetic-theory type hydrodynamic models to describe more realistic systems. In addition to the ordering and crystallization/melting, as described through g_Q instead of the classical Enskog $g_E = g_2$, a few simple, tractable correction terms were proposed that take into account the new physics and the corresponding parameters.

Firstly, elasticity and reduced energy dissipation during multi-particle collisions are accounted for through I_c from Eq. (52), involving an exponential correction factor that depends on the ratio of contact duration and time between contacts $\tau_c = t_c/t_n$. This correction only affects the energy dissipation rate in our model.

Friction activates the rotational degrees of freedom and therefore requires evolution equations also for the rotational degrees of freedom, with all the cross-talk terms and factors between the degrees of freedom. Only in special limit cases of large or small friction effective coefficients of restitution can be used, while otherwise, for realistic granular matter, complicated implicit equations must be solved.

Repulsive long-range forces and the reduced energy dissipation rate are accounted for by $I_{\rm rep}$ from Eq. (58). Attractive long-range forces and a somewhat increased energy dissipation rate is modeled through $I_{\rm atr}$ from Eq. (59). Both correction terms involve a Boltzmann-like exponential dependent on the ratio of energy of the repulsive/attracting potential and the kinetic (granular temperature) fluctuating energy. Like the elasticity, in our model, the long range interactions only affect the dissipation rate.

Wet granular systems were discussed elsewhere [31], but similar behavior as for attracting potentials was reported: The attraction is mediated through liquid bridges and the corresponding energy required for separation can be related to the granular temperature.

For bi- and poly-disperse systems, our study indicates that the equations of state can be expressed as functions of the moments of the size distributions [75, 115, 234] which in some special situations eliminates one parameter. For example, bi- and polydisperse systems are described by the same $g_\mathcal{A}$, which is only a function of the non-dimensional width of the size distribution. This prediction was never tested for other transport coefficients to our knowledge.

Furthermore, the issues of strong dissipation, size distributions, and non-spherical particles were discussed briefly and a few references were given as a starting-point for further literature search. Eventually, the differences between 2D and 3D phenomenology were introduced, rendering this review quantitative for 2D and qualitative for 3D.

8 Conclusion and Outlook

The basic idea of this study is to use the conservation equations for mass, momentum and energy, and to start with the constitutive relations provided by the mighty framework of kinetic theory. This leads to perfect quantitative theoretical predictions for smooth hard sphere simulation results at low and moderate densities and in the elastic limit.

Corrections and improvements are adapted to the constitutive relations for the transport coefficients, assuming that the conservation/balance equations for mass, momentum and energy are valid (and complete). *All corrections are applied to the pre-factors (transport coefficients) of the partial differential equations.* In this study we show results on how far one can get with this approach – with promising perspectives for further improvements.

For our extension of the dissipative hard-sphere model, the two most important corrections, in our opinion, are a pair-correlation function g_Q, that is valid at all densities and a new material parameter t_c, that accounts for possible multi-particle interactions and elasticity in the framework of the so-called TC model. The former accounts for crystallization and excluded volume effects, while the latter allows us to define concepts like "potential energy" and multi-particle collisions – with the related reduced energy dissipation.

Also other physical phenomena (e.g., long range forces) strongly affect the energy dissipation rate. Therefore, we postpone more detailed corrections of other transport coefficients to further studies.

New, very careful experiments are needed to achieve validation in order to enhance progress in this direction. The complexity of the theoretical model has to be increased step by step – and at each step experimental (and numerical) validation is needed.

References

1. J. Schwedes. *Fließverhalten von Schüttgütern in Bunkern.* Verlag Chemie, Weinheim, 1968.
2. P. K. Haff. Grain flow as a fluid-mechanical phenomenon. *J. Fluid Mech.*, 134:401–430, 1983.
3. C. S. Campbell and A. Gong. The stress tensor in a two-dimensional granular shear flow. *J. Fluid Mech.*, 164:107, 1986.
4. R. M. Nedderman. *Statics and kinematics of granular materials.* Cambr. Univ. Press, Cambridge, 1992.
5. A. Mehta, editor. *Granular Matter.* Springer, Berlin, 1994.
6. H.-B. Mühlhaus, editor. *Continuum Models for Materials with Microstructure.* Wiley, New York, 1995.
7. I. Vardoulakis and J. Sulem. *Bifurcation analysis in geomechanics.* Chapman & Hall, London, 1995.
8. D. C. Rapaport. *The Art of Molecular Dynamics Simulation.* Cambridge University Press, Cambridge, 1995.
9. D. E. Wolf and P. Grassberger, editors. *Friction, Arching and Contact Dynamics.* World Scientific, Singapore, 1997.
10. R. P. Behringer and J. T. Jenkins, editors. *Powders & Grains 97*, Rotterdam, 1997. Balkema.
11. H. J. Herrmann, J.-P. Hovi, and S. Luding, editors. *Physics of dry granular media - NATO ASI Series E 350*, Dordrecht, 1998. Kluwer Academic Publishers.
12. S. Luding. *Die Physik trockener granularer Medien.* Logos Verlag, Berlin, 1998. Habilitation thesis (in german), ISBN 3-89722-064-4.
13. C. Bizon, M. D. Shattuck, J. B. Swift, and H. L. Swinney. Transport coefficients for granular media from molecular dynamics simulations. *Phys. Rev. E*, 60(4):4340–4351, 1999.
14. T. Pöschel and S. Luding, editors. *Granular Gases*, Berlin, 2001. Springer. Lecture Notes in Physics 564.
15. P. A. Vermeer, S. Diebels, W. Ehlers, H. J. Herrmann, S. Luding, and E. Ramm, editors. *Continuous and Discontinuous Modelling of Cohesive Frictional Materials*, Berlin, 2001. Springer. Lecture Notes in Physics 568.

16. Y. Kishino, editor. *Powders & Grains 2001*, Rotterdam, 2001. Balkema.

17. L. E. Silbert, D. Ertas, G. S. Grest, T. C. Halsey, and D. Levine. Granular flow down an inclined plane: Bagnold scaling and rheology. *Phys. Rev. E*, 64:051302, 2002.

18. T. Murakami, T. Shimida, S. Yukawa, and N. Ito. Energy transport in multiphase system. *J. Phys. Soc. Japan*, 72(5):1049–1056, 2003.

19. T. Pöschel and N. V. Brilliantov, editors. *Granular Gas Dynamics*. Springer, Berlin, Germany, 2003.

20. H. Hinrichsen and D. E. Wolf, editors. *The Physics of Granular Media*. Wiley VCH, Weinheim, Germany, 2004.

21. T. Ishiwata, T. Murakami, S. Yukawa, and N. Ito. Particle dynamics simulations of the navier-stokes flow with hard disks. *Int. J. Mod. Phys. C*, 15:1413, 2004.

22. T. Pöschel and T. Schwager. *Computational Granular Dynamics*. Springer, Berlin, 2005.

23. R. Garcia-Rojo, H. J. Herrmann, and S. McNamara, editors. *Powders and Grains 2005*. Balkema, Leiden, Netherlands, 2005.

24. R. Garcia-Rojo, S. Luding, and J. J. Brey. Transport coefficients for dense hard-disk systems. *Phys. Rev. E*, 74(6):061305, 2006.

25. I. S. Aranson and L. S. Tsimring. Patterns and collective behavior in granular media: Theoretical concepts. *Rev. Mod. Phys.*, 78(2):641–692, 2006.

26. N. Mitarai and F. Nori. Wet granular materials. *Advances in Physics*, 55(1-2):1–45, 2006.

27. A. Donev, F. H. Stillinger, and S. Torquato. Configurational entropy of binary hard-disk glasses: Nonexistence of an ideal glass transition. *J. Chem. Phys.*, 127(12):124509, 2007.

28. T. Shinbrot, N. H. Duong, M. Hettenbach, and L. Kwan. Coexisting static and flowing regions in a centrifuging granular heap. *Granular Matter*, 9(5):295–307, 2007.

29. K. A. Reddy and V. Kumaran. Applicability of constitutive relations from kinetic theory for dense granular flows. *Phys. Rev. E*, 76(6):061305, 2007.

30. I. S. Aranson, L. S. Tsimring, F. Malloggi, and E. Clément. Nonlocal rheological properties of granular flows near a jamming limit. *Phys. Rev. E*, 78(3):031303, 2008.

31. A. Fingerle and S. Herminghaus. Equation of state of wet granular matter. *Physical Review E*, 77(1):011306, 2008.

32. K. van der Weele. Granular gas dynamics: how Maxwell's demon rules in a non-equilibrium system. *Contemporary Physics*, 49(3):157–178, 2008.

33. R. Brewster, L. E. Silbert, G. S. Grest, and L. J. Levine. Relationship between interparticle contact lifetimes and rheology in gravity-driven granular flows. *Phys. Rev. E*, 77(6):061302, 2008.

34. H. P. Zhu, Z. Y. Zhou, R. Y. Yang, and A. B. Yu. Discrete particle simulation of particulate systems: A review of major applications and findings. *Chem. Eng. Science*, 63(23):5728–5770, 2008.

35. J. W. Dufty, A. Baskaran, and J. J. Brey. Linear response and hydrodynamics for granular fluids. *Phys. Rev. E*, 77(3):031310, 2008.

36. J. J. Brey, M. J. Ruiz-Montero, and A. Dominguez. Shear state of freely evolving granular gases. *Phys. Rev. E*, 78(4):041301, 2008.

37. M. Nakagawa and S. Luding, editors. *Powders and Grains 2009*. American Institute of Physics (AIP), Golden, Colorado, USA, 2009. Confernce Proceedings #1145, ISBN 978-0-7354-0682-7.

38. I. Goldhirsch and G. Zanetti. Clustering instability in dissipative gases. *Phys. Rev. Lett.*, 70(11):1619–1622, 1993.

39. S. McNamara. Hydrodynamic modes of a uniform granular medium. *Phys. Fluids A*, 5(12):3056 – 3070, 1993.

40. S. McNamara and W. R. Young. Dynamics of a freely evolving, two-dimensional granular medium. *Phys. Rev. E*, 53(5):5089–5100, 1996.

41. S. Luding. Clustering instabilities, arching, and anomalous interaction probabilities as examples for cooperative phenomena in dry granular media. *T.A.S.K. Quarterly, Scientific Bulletin of Academic Computer Centre of the Technical University of Gdansk*, 2(3):417–443, July, 1998.

42. S. Luding and S. McNamara. How to handle the inelastic collapse of a dissipative hard-sphere gas with the TC model. *Granular Matter*, 1(3):113–128, 1998. e-print cond-mat/9810009.

43. S. Luding and H. J. Herrmann. Cluster growth in freely cooling granular media. *Chaos*, 9(3):673–681, 1999.

44. S. Luding. Structures and non-equilibrium dynamics in granular media. *Comptes Rendus Academie des Science*, 3:153–161, 2002.

45. S. Luding. From microscopic simulations to macroscopic material behavior. *Computer Physics Communications*, 147:134–140, 2002.

46. S. Luding. Molecular dynamics simulations of granular materials. In H. Hinrichsen and D. E. Wolf, editors, *The Physics of Granular Media*, pages 299–324, Weinheim, Germany, 2004. Wiley VCH.

47. S. Luding. Structure and cluster formation in granular media. *Pramana-Journal of Physics*, 64(6):893–902, 2005.

48. T. Pöschel, N. V. Brilliantov, and T. Schwager. Transient clusters in granular gases. *J. Phys.-Cond. Matter*, 17(24):S2705–S2713, 2005.

49. F. Zamponi. Some recent theoretical results on amorphous packings of hard spheres. *Philosophical Magazine*, 87(3-5):485–495, 2007.

50. R. Delannay, M. Louge, P. Richard, N. Taberlet, and A. Vallance. Towards a theoretical picture of dense granular flows down inclines. *Nature Materials*, 6(2):99–108, 2007.

51. E. Khain and B. Meerson. Shear-induced crystallization of a dense rapid granular flow: Hydrodynamics beyond the melting point. *Phys. Rev. E*, 73(6):061301, 2006.

52. E. Khain. Hydrodynamics of fluid-solid coexistence in dense shear granular flow. *Phys. Rev. E*, 75(5):051310, 2007.

53. P. Richard, A. Valance, J. F. Metayer, P. Sanchez, J. Crassous, M. Louge, and R. Delannay. Rheology of confined granular flows: Scale invariance, glass transition, and friction weakening. *Phys. Rev. Lett.*, 101(24):248002, 2008.

54. E. Khain. Bistability and hysteresis in dense shear granular flow. *Europhys. Lett.*, 87:14001, 2009.

55. P. Eshuis, K. van der Weele, D. van der Meer, R. Bos, and D. Lohse. Phase diagram of vertically shaken granular matter. *Phys. Fluids*, 19(12):123301, 2008.

56. J. A. Carrillo, T. Pöschel, and C. Saluena. Granular hydrodynamics and pattern formation in vertically oscillated granular disk layers. *J. Fluid Mech.*, 597:119–144, 2008.

57. P. Eshuis, K. van der Weele, M. Alam, H. J. van Gerner, M. van der Hoef, H. Kuipers, S. Luding, D. van der Meer, and D. Lohse. Buoancy driven convection in vertically shaken granular matter: Experiments, numerics and theory. *submitted to ???*, ???(???):???, 2009.

58. V. Kumaran. Dense granular flow down an inclined plane: from kinetic theory to granular dynamics. *J. Fluid Mech.*, 599:121–168, 2008.

59. V. Zivkovic, M. J. Biggs, D. H. Glass, P. Pagliai, and A. Buts. Particle dynamics in a dense vibrated fluidized bed as revealed by diffusing wave spectroscopy. *Powder Technology*, 182(2):192–201, 2008.

60. J. M. C. Hutchinson and P. M. Waser. Use, misuse and extensions of "ideal gas" models of animal encounter. *Biological Reviews*, 82(3):335–359, 2007.

61. B. D. Lubachevsky. How to simulate billards and similar systems. *J. Comp. Phys.*, 94(2):255, 1991.

62. S. Miller and S. Luding. Event driven simulations in parallel. *J. Comp. Phys.*, 193(1):306–316, 2004.

63. T. P. C. van Noije, M. H. Ernst, and R. Brito. Ring kinetic theory for an idealized granular gas. *Physica A*, 251:266–283, 1998.

64. S. Miller and S. Luding. Cluster growth in two- and three-dimensional granular gases. *Phys. Rev. E*, 69:031305, 2004.

65. S. Miller. *Clusterbildung in granularen Gasen*. PhD thesis, Universität Stuttgart, 2004.

66. I. Goldhirsch. Rapid granular flows. *Annu. Rev. Fluid Mech.*, 35:267–293, 2003.

67. D. Serero, I. Goldhirsch, S. H. Noskowicz, and M.-L. Tan. Hydrodynamics of granular gases and granular gas mixtures. *J. Fluid Mech.*, 554:237–258, 2006.

68. James F. Lutsko. Transport properties of dense dissipative hard-sphere fluids for arbitrary energy loss models. *Phys. Rev. E*, 72(2):021306, 2005.

69. I. Goldhirsch. Probing the boundaries of hydrodynamics. In T. Pöschel and S. Luding, editors, *Granular Gases*, Lecture Notes in Physics 564, pages 79–99. Springer, Berlin, 2000.

70. S. Luding, M. Müller, and S. McNamara. The validity of "molecular chaos" in granular flows. In *World Congress on Particle Technology*, Davis Building, 165-189 Railway Terrace, Rugby CV21 3HQ, UK, 1998. Institution of Chemical Engineers. ISBN 0-85295-401-9.

71. I. Pagonabarraga, E. Trizac, T. P. C. van Noije, and M. H. Ernst. Randomly driven granular fluids: Collisional statistics and short scale structure. *Phys. Rev. E*, 65(1):011303, 2002.

72. N. Mitarai and H. Nakanishi. Velocity correlations in dense granular shear flows: Effects on energy dissipation and normal stress. *Phys. Rev. E*, 75(3):031305, 2007.

73. M. Alam and S. Luding. First normal stress difference and crystallization in a dense sheared granular fluid. *Phys. Fluids*, 15(8):2298–2312, 2003.

74. Meheboob Alam and Stefan Luding. Energy nonequipartition, rheology, and microstructure in sheared bidisperse granular mixtures. *Physics of Fluids*, 17:063303, 2005.

75. S. Luding and A. Goldshtein. Collisional cooling with multi-particle interactions. *Granular Matter*, 5(3):159–163, 2003.

76. G. Lois, A. Lemaitre, and J. M. Carlson. Emergence of multi-contact interactions in contact dynamics simulations of granular shear flows. *Europhys. Lett.*, 76(2):318–324, 2006.

77. J. T. Jenkins and R. W. Richman. Plane simple shear of smooth inelastic circular disks: the anisotropy of the second momnent in the dilute and dense limit. *J. Fluid Mech.*, 192:313, 1988.

78. I. Goldhirsch and N. Sela. Origin of normal stress differences in rapid granular flows. *Phys. Rev. E*, 54(4):4458, 1996.

79. E. Cosserat and F. Cosserat. *Theorie des Corps Deformables*. Herman et fils, Paris, 1909.

80. H. Schaefer. Das Cosserat-Kontinuum. *Zeitschrift für angewandte Mathematik und Mechanik*, 47(8):485–498, 1967.

81. M. Becker and W. Hauger. Granular material - an experimental realization of a plastic Cosserat continuum. In O. Mahrenholtz and A. Sawczuk, editors, *Poznan*, pages 23–39, Poland, 1982. Warszawa.

82. R. de Borst. Simulation of strain localization: A reappraisal of the Cosserat continuum. *Engng. Comp.*, 8:317–332, 1991.

83. E. M. Dawson and P. A. Cundall. Cosserat plasticity for modeling layered rock. In L. R. Myer, C.-F. Tsan, N. G. W. Cook, and R. E. Goodman, editors, *Fractured and Jointed Rock Masses*, pages 267–274, Rotterdam, 1995. Balkema.

84. A. S. J. Suiker, A. V. Metrikine, and R. de Borst. Comparisons of wave propagation characterisitcs of the cosserat continuum model and corresponding discrete lattice models. *Int. J. of Solids and Structures*, 38:1563–1583, 2001.

85. L. Srinivasa Mohan, K. Kesava Rao, and Prabhu R. Nott. A frictional Cosserat model for the slow shearing of granular materials. *J. Fluid Mech.*, 457:377–409, 2002.

86. N. P. Kruyt. Statics and kinematics of discrete cosserat-type granular materials. *Int. J. of Solids and Structures*, 40(3):511–534, 2003.

87. P. Steinmann. A micropolar theory of finite deformation and finite rotation multiplicative elastoplasticity. *Int. J. Solids & Structures*, 31:1063–1084, 1994.

88. P. Steinmann. Theory and numerics of ductile micropolar elastoplastic damage. *Int. J. Num. Meth. Engng.*, 38:583–606, 1995.

89. H.-B. Mühlhaus and P. Hornby. On the reality of antisymmetric stresses in fast granular flows. In N. A. Fleck and A. C. E. Cocks, editors, *IUTAM Symposium on Mechanics of Granular and Porous Materials*, pages 299–311. Kluwer Academic Publishers, 1997.

90. M. Lätzel, S. Luding, and H. J. Herrmann. From discontinuous models towards a continuum description. In P. A. Vermeer, S. Diebels, W. Ehlers, H. J. Herrmann, S. Luding, and E. Ramm, editors, *Continuous and Discontinuous Modelling of Cohesive Frictional Materials*, pages 215–230, Berlin, 2001. Springer.

91. S. Luding, M. Lätzel, and H. J. Herrmann. From discrete element simulations towards a continuum description of particulate solids. In A. Levy and H. Kalman, editors, *Handbook of Conveying and Handling of Particulate Solids*, pages 39–44, Amsterdam, The Netherlands, 2001. Elsevier.

92. S. Luding, M. Lätzel, W. Volk, S. Diebels, and H. J. Herrmann. From discrete element simulations to a continuum model. *Comp. Meth. Appl. Mech. Engng.*, 191:21–28, 2001.

93. S. D. C. Walsh and A. Tordesillas. A thermomechanical approach to the development of micropolar constitutive models of granular media. *Act. Mech.*, 167:145–169, 2004.

94. D. Lhuillier. Constitutive relations for steady flows of dense granular liquids. *Physica A*, 383:267–275, 2007.

95. J. T. Jenkins and F. Mancini. Balance laws and constitutive relations for plane flows of a dense, binary mixture of smooth, nearly elastic, circular discs. *J. Appl. Mech.*, 54:27–34, 1987.

96. N. Sela and I. Goldhirsch. Hydrodynamic equations for rapid flows of smooth inelastic spheres to Burnett order. *J. Fluid Mech.*, 361:41–74, 1998.

97. J. J. Brey, J. W. Dufty, C. S. Kim, and A. Santos. Hydrodynamics for granular flow at low density. *Phys. Rev. E*, 58(4):4638, 1998.

98. J. J. Brey and D. Cubero. Steady state of a fluidized granular medium between two walls at the same temperature. *Phys. Rev. E*, 57(2):2019–2029, 1998.

99. N. V. Brilliantov and T. Pöschel. *Kinetic Theory of Granular Gases*. Oxford University Press, Oxford, UK, 2004.

100. K. Saitoh and H. Hayakawa. Rheology of a granular gas under a plane shear. *Phys. Rev. E*, 75(2):021302, 2007.

101. H. S. Noskowicz, D. Serero, and I. Goldhirsch. Near exact constitutive relations for molecular and granular gases up to moderate densities. unpublished, 2009.

102. J. T. Jenkins and M. W. Richman. Kinetic theory for plane shear flows of a dense gas of identical, rough, inelastic, circular disks. *Phys. of Fluids*, 28:3485–3494, 1985.

103. N. Mitarai and H. Nakanishi. Bagnold scaling, density plateau, and kinetic theory analysis of dense granular flow. *Phys. Rev. Lett.*, 94:128001, 2005.

104. T. P. C. van Noije, M. H. Ernst, R. Brito, and J. A. G. Orza. Mesoscopic theory of granular fluids. *Phys. Rev. Lett.*, 79:411, 1997.

105. T. P. C. van Noije and M. H. Ernst. Velocity distributions in homogeneous granular fluids: the free and the heated case. *Granular Matter*, 1(2):57–64, 1998. e-print cond-mat/9803042.

106. P. Rosenau. Extending hydrodynamics via the regularization of the Chapman-Enskog expansion. *Phys. Rev. A*, 40(12):7193, 1989.

107. N. Sela, I. Goldhirsch, and S. H. Noskowicz. Kinetic theoretical study of a simply sheared two-dimensional granular gas to Burnett order. *Phys. Fluids*, 8(9):2337, 1996.

108. M. Slemrod. Constitutive relations for rapid granular flow of smooth spheres: generalized rational approximation to the sum of the Chapman-Enskog expansion. *J. Diff. Eqns.*, 169:549, 2001.

109. S. Jin and M. Slemrod. Regularization of the Burnett equations via relaxation. *J. Stat. Phys.*, 103(5/6):1009, 2001.

110. P. M. Reis, R. A. Ingale, and M. D. Shattuck. Crystallization of a quasi-two-dimensional granular fluid. *Phys. Rev. Lett.*, 96:258001, 2006.

111. Danie Els. First-order phase transition and the equation of state in a 2d granular fluid. arXiv:cond-mat/0610839, 2009.

112. S. Torquato. Nearest-neighbor statistics for packings of hard spheres and disks. *Phys. Rev. E*, 51:3170, 1995.

113. D. Henderson. A simple equation of state for hard discs. *Molec. Phys.*, 30(3):971–972, 1975.

114. W. F. Carnahan and K. E. Starling. Equation of state for nonattracting rigid spheres. *J. Chem. Phys.*, 51(2):635–636, 1969.

115. S. Luding and O. Strauß. The equation of state of polydisperse granular gases. In T. Pöschel and S. Luding, editors, *Granular Gases*, pages 389–409, Berlin, 2001. Springer. e-print cond-mat/0103015.

116. S. Luding. Global equation of state of two-dimensional hard sphere systems. *Phys. Rev. E*, 63:042201–1–4, 2001.

117. S. Luding and A. Santos. Molecular dynamics and theory for the contact values of the radial distribution functions of hard-disk fluid mixtures. *J. Chem. Phys.*, 121(17):8458–8465, 2004.

118. N. Ito. Polydispersity effect to the fluid-solid transition. *Int. J. of Mod. Phys. C*, 7(3):275–280, 1996.

119. T. Hamanaka and A. Onuki. Transitions among crystal, glass, and liquid in a binary mixture with changing particle-size ratio and temperature. *Phys. Rev. E*, 74(1):011506, 2006.

120. K. E. Daniels and R. P. Behringer. Hysteresis and competition between disorder and crystallization in sheared and vibrated granular flow. *Phys. Rev. Lett.*, 94(6):168001, 2005.

121. K. E. Daniels and R. P. Behringer. Characterization of a freezing/melting transition in a vibrated and sheared granular medium. *J. Stat. Mech. – Theory and Experiment*, 2006:P07018, 2006.

122. S. Torquato and F. H. Stillinger. Toward the jamming threshold of sphere packings: Tunneled crystals. *J. Appl. Phys.*, 102(9):093511, 2007.

123. D. Hong. Effect of excluded volume and anisotropy on granular statistics: "fermi" statistics and condensation. In T. Pöschel and S. Luding, editors, *Granular Gases*, Berlin, 2000. Springer Verlag.

124. D. C. Hong, P. V. Quinn, and S. Luding. The reverse brazil nut problem: Competition between percolation and condensation. *Phys. Rev. Lett.*, 86:3423–3426, 2001.

125. S. Torquato, T. M. Truskett, and P. G. Debenedetti. Is random close packing of spheres well defined? *Phys. Rev. Lett.*, 84(10):2064–2067, 2000.

126. A. Donev, S. Torquato, and F. H. Stillinger. Pair correlation function characteristics of nearly jammed disordered and ordered hard-sphere packings. *Phys. Rev. E*, 71(1):011105, 2005.

127. James F. Lutsko and Gregoire Nicolis. Theoretical evidence for a dense fluid precursor to crystallization. *Phys. Rev. Lett.*, 96(4):046102, 2006.

128. James F. Lutsko. Ginzburg-landau theory of the liquid-solid interface and nucleation for hard spheres. *Phys. Rev. E*, 74(2):021603, 2006.

129. L. Heymann and N. Aksel. Transition pathways between solid and liquid state in suspensions. *Phys. Rev. E*, 75(2):021505, 2007.

130. S. Luding. Liquid-solid transition in bi-disperse granulates. *Advances in Complex Systems*, 4(4):379–388, 2002.

131. M. Alam, P. Shukla, and S. Luding. Universality of shear-banding instability and crystallization in sheared granular fluids. *J. Fluid Mech.*, 615:292–321, 2008.

132. M. Otsuki and H. Hayakawa. Universal scaling for the jamming transition. *Progress of Theoretical Physics*, 121:647–655, 2009.

133. W. W. Wood. Note on the free volume equation of state for hard spheres. *J. Chem. Phys.*, 20:1334, 1952.

134. H. Kawamura. A simple theory of hard disk transition. *Prog. Theor. Physics*, 61:1584–1596, 1979.

135. J. G. Kirkwood, E. K. Maun, and B. J. Alder. Radial distribution functions and the equation of state of a fluid composed of rigid spherical molecules. *J. Chem. Phys.*, 18(8):1040–1047, 1950.

136. R. J. Buehler, Jr. R. H. Wentorf, J. O. Hirschfelder, and C. F. Curtiss. The free volume for rigid sphere molecules. *J. of Chem. Phys.*, 19(1):61–71, 1951.

137. E. L. Grossman, T. Zhou, and E. Ben-Naim. Towards granular hydrodynamics in two-dimensions. *Phys. Rev. E*, 55:4200, 1997.

138. B. Meerson, M. Diez-Minguito, T. Schwager, and T. Pöschel. Close-packed granular clusters: hydrostatics and persistent gaussian fluctuations. *Granular Matter*, 10(1):21–27, 2007.

139. O. Herbst, P. Müller, M. Otto, and A. Zippelius. Local equation of state and velocity distributions of a driven granular gas. *Phys. Rev. E*, 70:051313–1–14, 2004. e-print cond-mat/0402104.

140. S. Luding. Granular media: Information propagation. *Nature*, 435:159–160, 2005.

141. F. H. Stillinger and G. Debenedetti. Alternative view of self-diffusion and shear viscosity. *Phys. Chem. D*, 109(14):6604–6609, 2005.

142. S. McNamara and S. Luding. Energy flows in vibrated granular media. *Phys. Rev. E*, 58:813–822, 1998.

143. R. D. Wildman and J. M. Huntley. Novel method for measurement of granular temperature distributions in two-dimensional vibro-fluidised beds. *Powder Technology*, 113(1-2):14–22, 2000.

144. S. Aumaitre, J. Farago, S. Fauve, and S. McNamara. Energy and power fluctuations in vibrated granular gases. *Eur. Phys. J. B*, 42(2):255–261, 2004.

145. R. Cafiero, S. Luding, and H. J. Herrmann. Two-dimensional granular gas of inelastic spheres with multiplicative driving. *Phys. Rev. Lett.*, 84:6014–6017, 2000.

146. S. Luding. Driven granular gases. In T. Pöschel and N. V. Brilliantov, editors, *Granular Gas Dynamics*, pages 293–316, Berlin, Germany, 2003. Springer.

147. R. Cafiero, S. Luding, and H. J. Herrmann. Rotationally driven gas of inelastic rough spheres. *Europhys. Lett.*, 60(6):854–860, 2002.

148. J. S. Olafsen and J. S. Urbach. Clustering, order and collapse in a driven granular monolayer. *Phys. Rev. Lett.*, 81:4369, 1998. e-print cond-mat/9807148.

149. O. Herbst, R. Cafiero, A. Zippelius, H. J. Herrmann, and S. Luding. A driven two-dimensional granular gas with coulomb friction. e-print cond-mat/0501223, 2005.

150. R. Brito and M. H. Ernst. Extension of Haff's cooling law in granular flows. *Europhys. Lett.*, 43(15):497–502, 1998. e-print cond-mat/9807224.

151. R. Soto, M. Mareschal, and M. Malek Mansour. Non-linear analysis of the shearing instability in granular gases. *Phys. Rev. E*, 62:3836–3842, 2000. e-print cond-mat/0002408.

152. James F. Lutsko. Chapman-enskog expansion about nonequilibrium states with application to the sheared granular fluid. *Phys. Rev. E*, 73(2):021302, 2006.

153. M. Alam. Streamwise structures and density patterns in rapid granular couette flow: a linear stability analysis. *J. Fluid Mech.*, 553:1–32, 2006.

154. V. Garzo. Transport coefficients for an inelastic gas around uniform shear flow: Linear stability analysis. *Phys. Rev. E*, 73(2):021304, 2006.

155. M. Otsuki and H. Hayakawa. Spatial correlations in sheared isothermal liquids: From elastic particles to granular particles. *Phys. Rev. E*, 79(2):021502, 2009.

156. Olaf Herbst and Isaac Goldhirsch. Heat flux in shear granular gases. private communication, 2008.

157. P. E. Krouskop and J. Talbot. Anisotropic energy distribution in three-dimensional vibrofluidized granular systems. *Phys. Rev. E*, 69:061308, 2004.

158. D. van der Meer and P. Reimann. Temperature anisotropy in a driven granular gas. *Europhys. Lett.*, 74(3):384, 2006.

159. Emmanuel Azanza, Francois Chevoir, and Pascal Moucheront. Experimental study of collisional granular flows down an inclined plane. *J. Fluid Mech.*, 400:199–227, 1999.

160. GDR MiDi. On dense granular flows. *Eur. Phys. J. E*, 14:341–365, 2004.

161. K. Hutter and K. R. Rajagopal. On flows of granular materials. *Continuum Mech. Thermodyn.*, 6:81–139, 1994.

162. R. Tykhoniuk, J. Tomas, S. Luding, M. Kappl, L. Heim, and H.-J. Butt. Ultrafine cohesive powders: From interparticle contacts to continuum behavior. *Chem. Eng. Sci.*, 62(11):2843–2864, 2007.

163. J. D. Goddard. Material instability in complex fluids. *Annu. Rev. Fluid Mech.*, 35:113–133, 2003.

164. J. Javier Brey and M. J. Ruiz-Montero. Validity of the boltzmann equation to describe low-density granular systems. *Phys. Rev. E*, 69:011305, 2004.

165. I. Goldhirsch and T. P. C. van Noije. Green-Kubo relations for granular fluids. *Phys. Rev. E*, 61:3241–3244, 2000.

166. N. V. Brilliantov, T. Pöschel, W. T. Kranz, and A. Zippelius. Translations and rotations are correlated in granular gases. *Phys. Rev. Lett.*, 98(12):128001, 2007.

167. C. K. K. Lun, S. B. Savage, D. J. Jeffrey, and N. Chepurniy. Kinetic theories for granular flow: inelastic particles in couette flow and slightly inelastic particles in a general flowfield. *J. Fluid. Mech.*, 140:223–256, 1984.

168. J. W. Dufty, A. Santos, and J. J. Brey. Practical kinetic model for hard sphere dynamics. *Phys. Rev. Lett.*, 77(7):1270–1273, 1996.

169. J. J. Brey, J. W. Dufty, and A. Santos. Kinetic models for granular flow. *J. Stat. Phys.*, 97:281–322, 1999.

170. V. Garzó and J. W. Dufty. Dense fluid transport for inelastic hard spheres. *Phys. Rev. E*, 59(5):5895–5911, 1999.

171. Rosa Ramirez, D. Risso, R. Soto, and P. Cordero. Hydrodynamic theory for granular gases. *Phys. Rev. E*, 62(2):2521–2530, 2000. e-print cond-mat/0001050.

172. H. Hwang and K. Hutter. A new kinetic model for rapid granular flow. *Continuum Mech. Thermodyn.*, 7:357–384, 1995.

173. S. Chapman and T. G. Cowling. *The mathematical theory of nonuniform gases*. Cambridge University Press, London, 1960.

174. L. D. Landau and E. M. Lifschitz. *Physikalische Kinetik*. Akademie Verlag Berlin, Berlin, 1986.

175. S. Luding, E. Clément, A. Blumen, J. Rajchenbach, and J. Duran. Anomalous energy dissipation in molecular dynamics simulations of grains: The "detachment effect". *Phys. Rev. E*, 50:4113, 1994.

176. Z. Zhao, C. S. Liu, and B. Brogliato. Energy dissipation and dispersion effects in granular media. *Phys. Rev. E*, 78(3):031307, 2008.

177. D. Z. Zhang. Evolution of enduring contacts and stress relaxation in a dense granular medium. *Phys. Rev. E*, 71(4):041303, 2005.

178. Charles S. Campbell. Granular shear flows at the elastic limit. *Journal of Fluid Mechanics*, 465:261–291, 2002. doi:10.1017/S002211200200109X.

179. Charles S. Campbell. Stress controlled elastic granular shear flows. *J. Fluid Mech.*, 539:273–297, 2005. doi:10.1017/S0022112005005616.

180. S. Luding, E. Clément, J. Rajchenbach, and J. Duran. Simulations of pattern formation in vibrated granular media. *Europhys. Lett.*, 36(4):247–252, 1996.

181. S. Luding. Surface waves and pattern formation in vibrated granular media. In *Powders & Grains 97*, pages 373–376, Amsterdam, 1997. Balkema.

182. N. V. Brilliantov, F. Spahn, J. M. Hertzsch, and T. Pöschel. Model for collisions in granular gases. *Phys. Rev. E*, 53(5):5382, 1996.

183. J. T. Jenkins. Dense shearing flows of inelastic discs. *Phys. Fluids*, 18(10):103307, 2006.

184. J. J. Brey, J. W. Dufty, and A. Santos. Dissipative dynamics for hard spheres. *J. Stat. Phys.*, 87(5/6):1051–1067, 1997.

185. J. J. Brey and D. Cubero. Hydrodynamic transport coefficients of granular gases. In T. Pöschel and S. Luding, editors, *Granular Gases*, pages 59–78, Berlin, 2001. Springer.

186. K. Saitoh and H. Hayakawa. Note on transport coefficients. Private Communication, 2009.

187. A. Santos, J. M. Montanero, J. Dufty, and J. J. Brey. Kinetic model for the hard-sphere fluid and solid. *Phys. Rev. E*, 57(2):1644, 1998.

188. E. Trizac and J. P. Hansen. Dynamic scaling behavior of ballistic coalescence. *Phys. Rev. Lett.*, 74(21):4114–4117, 1995.

189. E. Trizac and J. P. Hansen. Dynamics and growth of particles undergoing ballistic coalescence. *J. Stat. Phys.*, 82:1345–1370, 1996.

190. P. C. Johnson and R. Jackson. Frictional-collisional constitutive relations for granular materials, with application to plane shearing. *J. Fluid. Mech.*, 176:67, 1987.

191. S. Luding. Granular materials under vibration: Simulations of rotating spheres. *Phys. Rev. E*, 52(4):4442, 1995.

192. N. Mitarai, H. Hayakawa, and H. Nakanishi. Collisional granular flow as a micropolar fluid. *Phys. Rev. Lett.*, 88:174301, 2002.

193. O. Herbst, R. Cafiero, A. Zippelius, H. J. Herrmann, and S. Luding. A driven two-dimensional granular gas with coulomb friction. *Physics of Fluids*, 17(10):107102, 2005.

194. B. H. Ng, Y. Ding, and M. Ghadiri. Assessment of the kinetic-frictional model for dense granular flow. *Particuology*, 6:50–58, 2008.

195. S. McNamara and S. Luding. Energy nonequipartition in systems of inelastic, rough spheres. *Phys. Rev. E*, 58:2247–2250, 1998.

196. A. Barrat, E. Trizac, and J. N. Fuchs. Heated granular fluids: the random restitution coefficient approach. *Eur. Phys. J. E*, 5(2):161–170, 2001. e-print cond-mat/0101158.

197. A. Barrat and E. Trizac. Random inelasticity and velocity fluctuations in a driven granular gas. *Eur. Phys. J. E*, 11(1):99–104, 2003. LM 8381; e-print cond-mat/0205546.

198. J. T. Jenkins and C. Zhang. Kinetic theory for identical, frictional, nearly elastic spheres. *Physics of Fluids*, 14(3):1228–1235, 2002.

199. I. Goldhirsch, S. H. Noskowicz, and O. Bar-Lev. Weakly frictional granular gases. In S. P. Hoogendoorn, S. Luding, P. H. L. Bovy, M. Schreckenberg, and D. E. Wolf, editors, *Traffic and Granular Flow '03*, Berlin Heidelberg, 2005. Springer.

200. I. Goldhirsch, S. H. Noskowicz, and O. Bar-Lev. Nearly smooth granular gases. *Phys. Rev. Lett.*, 95(6):068002, 2005.

201. D. K. Yoon and J. T. Jenkins. Kinetic theory for identical, frictional, nearly elastic disks. *Phys. Fluids*, 17(8):083301, 2005.

202. S. F. Foerster, M. Y. Louge, H. Chang, and K. Allia. Measurements of the collision properties of small spheres. *Phys. Fluids*, 6(3):1108–1115, 1994.

203. O. Herbst, M. Huthmann, and A. Zippelius. Dynamics of inelastically colliding spheres with Coulomb friction: Relaxation of translational and rotational energy. *Granular Matter*, 2(4):211–219, 2000. e-print cond-mat/9911306.

204. D. E. Wolf, T. Scheffler, and J. Schäfer. Granular flow, collisional cooling and charged grains. *Physica A*, 274(1-2):171–181, 1999.

205. T. Scheffler and D. E. Wolf. Collisional cooling in charged granular gases. *Granular Matter*, 4(3):103–113, 2002.

206. M.-K. Müller. *Long-Range Interactions in Dilute Granular Systems*. PhD thesis, University of Twente, Netherlands, 2008.

207. M. Müller and S. Luding. Homogeneous cooling with repulsive and attractive long-range interactions. In M. Nakagawa and S. Luding, editors, *Powders and Grains 2009*, pages 493–497, Golden, Colorado, USA, 2009. AIP Conf. Proc. #1145.

208. A. Fingerle, K. Roeller, K. Huang, and S. Herminghaus. Phase transitions far from equilibrium in wet granular matter. *New Journal of Physics*, 10:053020, 2008.

209. A. Santos, S. B. Yuste, and M. L. de Haro. Contact values of the radial distribution functions of additive hard-sphere mixtures in d dimensions: A new proposal. *J. Chem. Phys.*, 117:5785–5793, 2002.

210. M. Alam, J. T. Willits, B. O. Arnarson, and S. Luding. Kinetic theory of a binary mixture of nearly elastic disks with size and mass-disparity. *Physics of Fluids*, 14(11):4085–4087, 2002.

211. M. Alam and S. Luding. How good is the equipartition assumption for transport properties of a granular mixture. *Granular Matter*, 4(3):139–142, 2002.

212. M. Alam and S. Luding. Rheology of bidisperse granular mixtures via event driven simulations. *J. Fluid Mech.*, 476:69–103, 2003.

213. A. Santos, S. B. Yuste, and M. L. de Haro. Contact values of the particle-particle and wall-particle correlation functions in a hard-sphere polydisperse fluid. *J. Chem. Phys.*, 123(23):234512, 2005.

214. M. Dijkstra and D. Frenkel. Evidence for entropy-driven demixing in hard-core fluids. *Phys. Rev. Lett.*, 72(2):298–300, 1994.

215. L. Trujillo and H. J. Herrmann. Hydrodynamic model for particle size segregation in granular media. *Physica A*, 330(3-4):519–542, 2003.

216. M. Alam, L. Trujillo, and H. J. Herrmann. Hydrodynamic theory for reverse brazil nut segregation and the non-monotonic ascension dynamics. *J. Stat. Phys.*, 124(2-4):587–623, 2006.

217. V. Garzo. Brazil-nut effect versus reverse brazil-nut effect in a moderately dense granular fluid. *Phys. Rev. E*, 78(2):020301, 2008.

218. S. Godoy, D. Risso, R. Soto, and P. Cordero. Rise of a brazil nut: A transition line. *Phys. Rev. E*, 78(3):031301, 2008.

219. M. Dijkstra and D. Frenkel. Phase separation in binary hard-core mixtures. *J. Chem. Phys.*, 101(4):3179–3189, 1994.

220. W. Vermöhlen and N. Ito. State diagram of polydisperse elastic-disk systems. *Phys. Rev. E*, 51(5):4325, 1995.

221. K. M. Aoki and N. Ito. Effect of size polydispersity on granular materials. *Phys. Rev. E*, 54(2):1990–1996, 1996.

222. J. Zhang, R. Blaak, E. Trizac, J. A. Cuesta, and D. Frenkel. Optimal packing of polydisperse hard-sphere fluids. *J. Chem. Phys.*, 110(11):5318–5324, 1999.

223. V. Garzo, C. M. Hrenya, and J. W. Dufty. Enskog theory for polydisperse granular mixtures. II. Sonine polynomial approximation. *Phys. Rev. E*, 76(3):031304, 2007.

224. A. Donev, I. Cisse, D. Sachs, E. Variano, F. H. Stillinger, R. Connelly, S. Torquato, and P. M. Chaikin. Improving the density of jammed disordered packings using ellipsoids. *Science*, 303(5660):990–993, 2004.

225. A. Donev, R. Connelly, F. H. Stillinger, and S. Torquato. Underconstrained jammed packings of nonspherical hard particles: Ellipses and ellipsoids. *Phys. Rev. E*, 75(5):051304, 2007.

226. A. Donev, S. Torquato, and F. H. Stillinger. Neighbor list collision-driven molecular dynamics simulation for nonspherical hard particles. i. algorithmic details. *J. Comp. Phys.*, 202(2):737–764, 2007.

227. A. Donev, S. Torquato, and F. H. Stillinger. Neighbor list collision-driven molecular dynamics simulation for nonspherical hard particles. ii. applications to ellipses and ellipsoids. *J. Comp. Phys.*, 202(2):765–793, 2007.

228. A. Schinner. Fast algorithms for the simulations of polygonal particles. *Granular Matter*, 2(1):35–43, 1999.

229. F. Kun, G. A. D´Addetta, E. Ramm, and H. J. Herrman. Two-dimensional dynamic simulation of fracture and fragmention of solids. *Comp. Ass. Mech. Engng.*, 6:385–402, 1999.

230. L. Pournin, M. Weber, M. Tsukahara, J. A. Ferrez, M. Ramaioli, and T. M. Liebling. Three-dimensional distinct element simulation of spherocylinder crystallization. *Granular Matter*, 7(2-3):119–126, 2005.

231. A. Wouterse, S. Luding, and A. Philipse. On contact numbers in random rod packings. *Granular Matter*, 11:in press, 2009.

232. M. Mailman, C. F. Schreck, C. S. O'Hern, and B. Chakraborty. Jamming in systems composed of frictionless ellipse-shaped particles. *Phys. Rev. Lett.*, 102:255501, 2009.

233. Z. Zeravcic, N. Xu, A. J. Liu, S. R. Nagel, and W. van Saarloos. Excitations of ellipsoid packings near jamming. *Europhys. Lett.*, 87:26001, 2009.

234. M. Madadi, O. Tsoungui, M. Lätzel, and S. Luding. On the fabric tensor of polydisperse granular media in 2d. *Int. J. Sol. Struct.*, 41(9-10):2563–2580, 2004.